Supplemental Materials:

Contains Methods, Supplemenral text, Supplemental Figure Legend, Supplemental References.

Supplemental Methods:

Experimental model of acute alcoholic steatohepatitis (the NIAAA model: chronic ethanol Lieber-DeCarlie diet + single alcohol binge)[1]. Mice (♂ C57BL/6, 12 w old, n=7/group, 2 independent experiments) were fed with a liquid diet containing 5% ethanol for 10 days, and at day 11 gavaged with a single dose of ethanol (5g/kg, 20% ethanol), and sacrificed 9 h post binge. Control littermates were pair-fed with 9 g maltose dextrin/kg of body weight.

Experimental model of chronic alcoholic steatohepatitis (chronic ethanol Lieber-DeCarlie diet + weekly binges[2]**)**: Mice (♂ C57BL/6, 12 w old, n=8-10/group, 2 independent experiments) were fed *ad libitum* for 2 weeks with a liquid "Western diet" (high in cholesterol (1%) and saturated fat (27% Cal), followed by 8 weeks of an ethanol-containing Western diet. Ethanol intake was gradually increased from 1% (w/v) on day 1 to 4.5% (w/v) on day 12 until the end of 8th week of feeding. From the second week of ethanol feeding, a weekly binge dose of ethanol (gradually increased from 3.5 g/kg to 4.5 g/kg) was given via a stomach tube and repeated 7 times. Mice were sacrificed 24 h after the alcohol-binge treatment.

Detection of serum IL17A in patients with severe alcohol use disorder. Healthy controls (n=18, non-smokers without underlying medical illnesses) were recruited at the Roudebush Veterans Administration Medical Center (Indianapolis, IN). Excessive drinkers (n=57, defined by NIH/NIAAA guideline: ≥ 21 years of age; > 4 standard drinks/day (or >14 drinks/week) in men; and > 3 drinks/day (or >7 drinks/week) in women[3] were recruited from Fairbanks Drug and Alcohol Treatment Center (Indianapolis, IN). Exclusion criteria: active and chronic medical diseases; history of chronic HCV/HBV, or systemic infection within 4 weeks prior to the study. The Time Line Follow-Back questionnaire was used to determine the quantity of alcohol consumption over the 30-day period before the enrollment[4,5]. Blood samples were obtained for complete blood count and hepatic panel, serum was analyzed using IL-17A ELISA kit (R&D Systems, #D1700). Excessive drinkers were further dichotomized into those with normal (ALT<40 U/L) and elevated ALT (ALT≥ 40 U/L). The study was approved by the Indiana University Purdue University Institutional Review Board, the Research and Development Committee at Roudebush VA, and Fairbanks Drug and Alcohol Treatment Center. All participants provided written informed consent, patient information is provided in Suppl. Table 1 and 2.

Serum ALT and AST measurement: The serum concentrations of alanine aminotransferase (ALT) and aspartate amino-transaminase (AST) were evaluated according to the kit protocol (Fisher Infinitv, #ALT NC9511745).

Histology and immunohistochemistry: Immunohistochemistry was performed on formalin-fixed tissues using anti-α-SMA Ab (Abcam, #ab5694 1:200), anti-desmin Ab (Fisher Neuromarkers, #RB-9014-P0 1:100), anti-F4/80 Ab (eBioscience, #14-4801-82 1:100), anti-4-HNE Ab (Alpha Diagnostic international Inc., #HNE11-S 1:100), anti-GFAP Ab (BD Bioscience, 556330 1:1000), anti-Iba1 Ab (Abcam, ab5076 1:200), anti-Albumin Ab (Biorad, AHP1478 1:100), anti-Caspase 3 Ab (Abcam, ab13847 1:100), Zo-1 (BD Bioscience, 610966 1:100), and DAPI (Invitrogen, D21490). HRP or fluorescein conjugated secondary antibodies were obtained from Invitrogen or Vector Immpress (anti-rabbit MP-7401 and anti-rat MP-7444). Immunoreactivity was visualized by 3,3'-diaminobenzidine tetrahydrochloride staining (Vector Laboratories). Tissues were counterstained with Hematoxylin. Images of seven non-overlapping fields were randomly selected and taken using Olympus microscope, and quantified using Image J (https://imagej.net/docs/examples/stained-sections/index.html), and (https://imagej.nih.gov/ij/developer/macro/macros.html).

Quantitative RT-PCR was performed using a StepOnePlus Real-Time PCR system (Applied Biosystems). Whole livers, whole brains, frontal cortex, hippocampus, or cerebellum were dissected and snap-frozen. Total RNA was isolated using RNeasy columns (Qiagen). Expression level of selected genes was calculated vs housekeeping gene HPRT using the ΔΔ CT method (Invitrogen). The data are fold change (vs controls) or relative mRNA level (vs controls), mean + SD, * $p < 0.05$, ** $p < 0.01$

Phenotyping of IL17A producing cells in the livers of IG alcohol-fed mice. Murine hepatic single cell suspension (generated by pressing the livers through a 70-μm cell strainer, Becton Dickinson) was resuspended in 35% isotonic Percoll (17-0891-01; 7.2% 10X PBS, and 1.2% sodium bicarbonate, GE Healthcare) and DMEM (SH30022.01; Hyclone), then centrifuged for 15 min at 2000 rpm. Cell pellet was broken down and treated with red blood cell lysing solution (5 ml for 7 min at RT, R7757; Sigma), and then washed twice with DMEM supplemented with 2% FBS (HyClone). The non-parenchymal cells (NPCs) were analyzed by flow cytometry for expression of intracellular cytokines. The intracellular cytokine production was assessed by BD Cytofix/Cytoperm Plus Fixation/Permeabilization Kit with BD GolgiPlug protein transport inhibitor containing brefeldin A (BD, 555028). NPCs were fractionated in a 12 well cell culture plate at concentration of 1 x 10^6 cells/well. The cells were cultured for 6 hours at 37^{o}C in complete RPMI 1640 (Hyclone, SH30027.01) media supplemented with 10%FBS, sodium pyruvate, L-Glut, Pen/Strep, Hepes, non-essential amino acids, 2-ME, in the presence of PMA 10 ng/ml (P8139; Sigma), ionomycin 500 ng/ml (I-0634; Sigma), and Golgi Plug 1μl/ml. At the end of the incubation, cells were harvested, washed two times in FACS buffer (PBS containing 0.02% NaN3 and 2% FCS) and blocked with Fc block (Purified Rat Anti-Mouse CD16/CD32 (93; Biolegend)) and then stained with fluorescent conjugated mABs against surface antibody markers CD4 (GK1.5; Biolegend), TCRβ (H57-597; Biolegend) and αGal/Cer/mCD1d tetramer. The PE conjugated αGalCer/mCD1d tetramer was produced in the laboratory from High Five™ insect cells (BTITN-5B1-4) using the Baculovirus Expression Vector System (ThermoFisher Scientific). After surface staining, cells were fixed and permeabilized and stained for

intracellular cytokines: IFN-γ (XMG1.2; eBioscience), IL-4 (BVD6-24G2; eBioscience), IL-17 (eBio17B7; eBioscience), IL-22 (IL22JOP, eBioscience) according to the manufacturer's kit instructions. The acquired data was analyzed using FlowJo software by gating on the $CD4^+/TCR\beta^+$ cells.

The whole brain MRI. Dependent and non-dependent mice were treated with the anti-IL-17A Ab or IgG, brains were perfused with a fixative 7 days after the final administration of IL17A ab (3 days after the last 2BC session). Macrostructural changes of the brain were evaluated by volumetric analysis of T2-weighted MRI scans of the whole brains.

Western Blotting analysis: The primary antibodies and dilutions were as follows: anti-CYP2E1 Ab (Fisher ab1252 1:3000), anti-IL17A Ab (eBiosciences 14-7175-81 1:1000), and anti-β-actin Ab (Sigma, a5441, 1:5000).

***In situ* hybridization:** IL17A mRNA was detected in samples using RNAscope *in situ* RNA hybridization. Livers and brains were formalin fixed and paraffin embedded. 4μm tissue sections were collected in an RNase-fee manner, dried overnight, backed (for 32 min at 60°C), de-paraffinized, and subjected to antigen retrieval (two sequential treatments with protease at 65°C and 75°C for 12 min each, Advanced Cell Diagnostics). *In situ* hybridization (ISH) was performed on a Ventana Discovery Ultra automated stainer; IL17A-specific RNA target z-DNA probe sets[6] were provided by the manufacturer (Ventana Medical Systems, Tucson, USA). Following amplification, horseradish

peroxidase-labeled mRNA was visualized using 3,3' diaminobenzidine (DAB), sections counterstained with hematoxylin.

Isolation of hepatocytes and Kupffer cells: Livers were perfused using pronase/collagenase method. Single-cell suspensions were centrifuged at 50g for 1 min to pellet the hepatocyte fraction. The remaining non-parenchymal cell fraction was collected. Kupffer cells were isolated by gradient centrifugation (15% Nycodenz) followed by magnetic sorting with anti-CD11b magnetic beads (Miltenyi Biotec)[7].

Gene expression profiling of murine hepatocytes and Kupffer cells: Isolated primary hepatocytes and Kupffer cells were subjected to RNA-Seq. Hippocampus was dissected from brains of Air and CIE ± anti-IL17A Ab mice. Strand specific mRNA-sequencing libraries (polyA+) were generated using Illumina's TruSeq stranded mRNA library prep kits, and sequenced on an Illumina HiSeq2500 to a depth of approximately 25 million reads. Sequencing reads were aligned to the mouse genome (NCBI MGSCv37, mm9) using STAR[8]. Gene expression levels, gene ontology, and clustering were performed using HOMER and Cluster3.0/Java Tree View[9]. Differentially expressed genes were identified using edgeR[10].

Isolation of astrocytes and microglial cells: Primary astrocytes were isolated from the brains of the 4 postnatal pups (P1) using DNase (300g/ml, Roche) and trypsin (0.25%, Sigma-Aldrich) digestion method, combined, cultured and sort purified[11]. Primary microglial cells were isolated using anti-CD11b Ab-conjugated magnetic beads (Miltenyi

Biotech). Cells (5 x 10^5) were cultured in DMEM with 10% FBS, and treated with IL17A cytokine (5ng/ml) or PBS for 6 h, harvested and analyzed by qRT-PCR.

Gene experession profiling of murine astrocytes: Primary astrocytes (5 x 10^5 cells) were stimulated with ± IL-1β (5ng/ml), TGF-β1(5ng/ml) or vehicle for 24 h, harvested, and mRNA was purified using RNAeasy columns (Qiagen); and 160 ng of purified RNA per sample was labeled using the LRILAK PLUS, 2-color, low RNA input Linear Amplification kit and hybridized to a Whole Mouse Genome Microarray 4X44 K 60mer slide according to the manufacturer's instructions (Agilent, Santa Clara, CA). Slides were scanned using the Agilent GZ505B Scanner and analyzed using the Gene Spring Software (Agilent). Differentially regulated genes were defined as those with significant absolute expression (>9-$\log_2$ intensity value) and exhibiting 2-fold compared with the maximal value in all other samples. The data are representative of 2 independent experiments.

Enzyme linked immunosorbent assay (ELISA): Serum and cerebrospinal fluid (CSF)[12] were collected, the levels of IL17A (Biolegend, #432501), TNF-α (Biolegend, #430901), IL-1β (Biolegend, #432601), TGF-β1 (eBioscience, #88-8350-22), IL-6 (Biolegend, #431301) were measured[13]. The concentration of CSF cytokines was calculated as ng/ml and normalized by total protein concentration.

Vascular permeability assay: Air, and CIE mice were injected with Evans blue solution (30 mg/kg, i.v., Sigma)[14] immediately after the last vapor session, and sacrificed 1 h later.

Tissues were perfused with 20 ml PBS. Evans blue dye was extracted in 0.5 ml formamide (55°C, 24 h). Yield of dye was measured spectrophotometrically (λ = 610 nm), the data are ng/mg of brain tissue.

Fecal sample collection and DNA extraction: Microbial DNA was extracted from mouse fecal samples using the Powersoil DNA Isoltion Kit (Qiagen), following manufacturer's instructions. Extracted DNA was quantified using the Nanodrop 1000 Spectrophotometer (Thermo Fisher Scientific).

16S rRNA Amplification and Library Preparation: Protocols from the Earth Microbiome Project were followed for DNA amplification and library preparations[15]. The V4 region of the 16S ribosomal RNA gene was amplified using the primers: GTGYCAGCMGCCGCGGTAA and GGACTACNVGGGTWTCTAAT. Libraries were sequenced on the Illumina MiSeq platform.

16S rRNA Data Analysis: Sequence data was de-multiplexed, quality-filtered and clustered with QIIME 2. Grouping of operational taxonomic units (OTUs) was done using a similarity threshold of 97% and OTU assignment was done by closed-reference picking using the Greengenes reference dataset (version 13.8). This was used to generate OTU bar-plots of microbial composition. In addition, Bray-Curtis distances were calculated and used to generate principal coordinate analysis visualizations.

Supplemental Text:

1. Analysis of liver pathology in mice subjected to experimental models of ALD (supports Figure 1A) was performed by a pathologist in a double blinded manner. Mice with acute alcoholic steatohepatitis developed neither steatosis (grade 0: steatosis is < 5%) nor fibrosis. Mice with chronic alcoholic steatohepatitis developed grade 1-2 steatosis (median grade 1). Steatosis was primarily observed in hepatocytes in zone 2 (versus the typical centrizonal/zone 3 observed in patients). These mice also exhibited lobular inflammation (grade 1-2), minimal fibrosis (stage 0-1), no hepatocyte ballooning or Mallory-Denk bodies. Mice with alcoholic liver fibrosis developed steatosis (grade 3) with highest fat concentration in zone 2 followed by zones 1 and 3, significant lobular inflammation (grade 2), hepatic fibrosis (stage 1-2), and spotty necrosis of hepatocytes, but no hepatocyte ballooning or Mallory-Denk bodies.

2. Experimental model of acute ASH in wt mice (supports Suppl. Figure 1) caused significant damage to hepatocytes (ALT 110 ± 32 IU/L, Supp. Figure 1A), mild hepatic inflammation, recruitment of neutrophils, upregulation of IL17A, IL17RA, and IL-23[1]. Expression of fibrogenic genes (Col1a1, α-SMA, TIMP1, Supp. Figure 1B) was not induced in these mice, suggesting that this model mimics initial stages of alcoholic steatohepatitis in patients, and can be used to study the onset of ALD.

3. Experimental model of chronic ASH in wt mice (supports Suppl. Figure 2**).** Chronic-multiple binge alcohol fed wt mice developed significant hepatocellular injury and

steatosis, as demonstrated by increased ALT (121 ± 30 U/I vs 60 U/I in the pair-fed mice, Suppl. Figure 2A), induction of oxidative stress (via induction of NOX4, p22 Phox, and p67 Phox, Suppl. Figure 2F), upregulation of hepatic triglycerides (↑2 fold), products of lipid peroxidation 4-HNE (↑3 fold) (Suppl. Figure 2B), and expression of adipogenic genes (increased expression of SREBP-1c, and suppression of PPARα, Suppl. Figure 2E). Increased flux of inflammatory cells (increase ↑2 fold vs pair-fed mice), including $Ly6G^+$ neutrophils (↑6 fold) and $F4/80^+$ Kupffer cells (↑2 fold) (Suppl. Figure 2B) was observed in livers of alcohol fed mice, and was associated with upregulation of pro-inflammatory cytokines IL-6 (↑2 fold), IL-1β (↑3.5 fold) (Suppl. Figure 2H), and neutrophil chemoattractant MIP-1 (↑10 fold) and MIP-2 (↑2.5 fold) (Suppl. Figure 2G), and TGF-β1 (↑1.5 fold, Suppl. Figure 2I), while expression of IL-8 and TNF-α was not significantly changed between alcohol- and pair-fed mice. Although hepatic expression of α-SMA (↑1.3 fold), Col1a1 (↑2.2 fold), and TIMP1 (↑5 fold) (Suppl. Figure 2I) were upregulated above the basal level, the number of $Desmin^+$ HSCs in livers of alcohol-fed mice was moderately increased (↑1.5 fold vs pair-fed mice, Suppl. Figure 2B), indicating that these mice exhibited activation of HSCs associated with the very onset of liver fibrosis, suggesting that this model of alcohol feeding recapitulates advanced alcoholic steatohepatitis similar to that observed in patients.

4. Experimental model of liver fibrosis in alcohol-fed wt mice (supports Suppl. Figure 3)**.** Wt mice (♂ C57BL/6, 12 w old) were surgically operated to insert intragastric catheter, and upon recovery (2 weeks) were subjected to intragastric (IG) alcohol feeding (Tsukamoto-French model)[16-19], pair-fed, or chow-fed. In comparison, chronic alcohol

fed mice + multiple binge, IG alcohol-fed mice developed severe hepatocellular injury, as shown by increased ALT (215 ± 51 U/I vs 80 ± 15 U/I in pair-fed mice, Figure 3A). Hepatic steatosis and the triglycerides content (↑1.5 fold vs pair-fed mice, Suppl. Figure 3B) were strongly increased in IG alcohol-fed mice, while expression of beta-oxidation genes (PPARα) was suppressed (↓2 fold, Suppl. Figure 3E). Induction of lipid peroxidation enzymes 4-HNE (↑3 fold, Suppl. Figure 3B) and TBARS (↑2 fold) was associated with reduced levels of the GSH (↓2 fold) (Suppl. Figure 3C and D), indicative of development of intrahepatic oxidative stress and severe liver injury. In support, we observed significant increase in expression of NOX1, NOX2, and p67 Phox (Suppl. Figure 3F). Unlike chronic-multiple binge alcohol fed mice (Suppl. Figure 2F), expression of hepatic NOX4 was not changed in IG alcohol-fed mice, indicating that differential expression of alcohol-induced genes depends on the regiment/duration of alcohol administration (similar to that observed in patients with different stages of ALD). In agreement, IG alcohol-fed mice developed severe fibrosis and inflammation, as shown by increased positive area of Sirius Red staining (↑3.5 fold vs pair-fed mice), and staining for F4/80$^+$ Kupffer cells (increase ↑3.5 fold) (Suppl. Figure 3B). We observed strong induction of hepatic α-SMA (↑6 fold), Col1a1 (↑14 fold), and TIMP1 (↑50 fold) in livers of IG alcohol-fed mice (Figure 2C), which correlated with increased number of activated Desmin$^+$ HSCs (↑2 fold vs pair-fed mice, Suppl. Figure 3B). Development of liver fibrosis in these mice was associated with release of profibrogenic factor TGF-β1 (↑7 fold, Figure 2C) and the variety of pro-inflammatory cytokines IL-6 (↑15 fold), IL-1β (↑15 fold), TNFα (↑15 fold) (Figure 2D), including chemoattractant MIP-1 (↑13 fold) and MIP-2 (↑16 fold) (Suppl. Figure 3G). Furthermore, expression of IL-8 and Ly6G was

not changed between IG alcohol- and pair-fed mice (Suppl. Figure 3G), suggesting that Kupffer cells (but no longer neutrophils) critically mediate progression from steatohepatitis to fibrosis at this stage of ALD. Non-parenchymal mononuclear cells were isolated from the livers of IG alcohol-fed mice, *in vitro* re-stimulated with PMA, expression of IL-17A was measured in $TCR\beta^{+}CD4^{+}$ cells using flow cytometry. Intracellular expression of IL17A was doubled in $TCR\beta^{+}CD4^{+}$ cells upon exposure to alcohol (vs pair-fed mice, Suppl. Figure 3G). The population of IL17A-expression $TCR\beta^{+}CD4^{+}$ cells did not express Il-22, or Il-4, and minimally expressed IFN-γ.

5. Activated astrocytes serve as a significant source of cytokines and chemokines (supports Suppl. Figure 7). In response to IL17A stimulation, microglial cells produce TGF-β1 and IL-1β (Suppl. Figure 7A). To determine the effect of microglia-derived cytokines on astrogliosis [20,21], cultured $GFAP^{+}F4/80^{-}$ astrocytes were *in vitro* stimulated with ± TGF-β1 or IL-1β. We confirmed that astrocytes do not express IL17A family of cytokines (IL17A, IL17B, IL17C, IL17F, except IL17D)[22], but express all three IL17A receptors (IL17RA, IL17RC and IL17RD, not shown). Cultured astrocytes highly expressed IL-11, IL-18, IL-27, IL-33 (and IL-33RA, not shown), TGF-α and β, tenascin C (Tnc), and IK cytokine mRNA (not shown), but did not express IL-1α or β, or TNF-α mRNA. Upon stimulation with IL-1β, astrocytes strongly induced the hallmark inflammatory response, hallmark complement; response to cytokines, response to toxic substances, regulation of cell-cell adhesion (see the GO enrichment profile, Suppl. Figure 7B), and serve as a significant source of pro-inflammatory cytokines and chemokines, such as CCL7 (↑ 400 fold vs vehicle), CCL2 (↑ 200 fold), IL-6 (↑ 20 fold), Cxcl1 (↑ 14

fold), and CCL5 (↑ 13 fold) (Suppl. Figure 7D). IL-1β-stimulated astrocytes also upregulated expression of IL-1R1, IL-10Rb, IL-13Ra, IL-15Ra, IL-4Ra mRNA (not shown), suggesting that IL-1β signaling exerts inflammatory responses in activated astrocytes (Suppl. Figure 7B). Different set of genes was induced in TGF-β1-stimulated astrocytes, and was associated with cellular response to growth factor stimulus, hallmark of TGF-β1 and TNF-α signaling, tissue morphogenesis, negative regulation of cell death (see the GO enrichment profile, Suppl. Figure 7C), strongly upregulated expression of TGF-β1 and TGFβRI, NOX4, PAI-1, TIMPs, fibronectin, IL-6, PDGFα and β, CTGF, IL-11, FGF2 and 18, several kinases (Irak2 and Jag1, Jun B), integrins (Itga 11, Itga 5 fibronectin receptor a, Itgb5), several members of actin and kinesin families (Suppl. Figure 7D). In addition, cultured astrocytes expressed glutamate receptors (mGluRs) that mediate neuron-astrocyte signaling (Suppl. Figure 7D). Under pathological conditions, neurodegeneration triggers expansion of reactive astrocytes, upregulation of TGF-β1, and mGluRs, which together generate neuroprotective effects[23]. Here we demonstrate TGF-β1 induced expression of glutamate transporters (Slc1a4, Slc20a1, Slc22a23, not shown) in astrocytes, in contrasts to IL-1β which suppressed expression of glutamate receptors Gria 1 and 4 in astrocytes, suggesting that IL-1β and TGF-β1 have opposing effects on glial-neuronal communication.

6. Alcohol-injured lungs are the source of circulating IL17A in alcohol-dependent mice (supports Suppl. Figure 12A-D). To identify the source of IL17A, livers, brains, and lungs of CIE and Air mice were examined. Since alcohol metabolism was deliberately blocked in the livers of CIE mice (by pyrazol administration) to maximize the effect of

alcohol on development of alcohol-dependence in mice, CIE mice were protected from alcohol-induced liver injury (Suppl. Figure 12A). Therefore, lungs served as a major source of IL17A in CIE mice (Suppl. Figure 12C). Similarly to IG alcohol-fed mice (Suppl. Figure 9C), IL17A was not expressed in the brains of CIE mice (Suppl. Figure 12B). In turn, IL17A mRNA was strongly induced (↑ 2 fold vs Air mice) in the lungs of CIE mice (Suppl. Figure 12C-D), suggesting the alcohol-injured lungs are the major source of IL17A in alcohol-dependent CIE mice. Upregulation of IL17A in the lungs of CIE mice (vs livers of IG alcohol-fed mice) was largely determined by the route of alcohol administration (vapor inhalation vs ingestion), demonstrating that development of alcohol-dependence in mice can be achieved in the absence of alcohol-induced liver injury.

Supplemental Figure Legend:

Suppl. Figure 1. Development of acute ASH is not attenuated in IL17ra$^{-/-}$ mice. **(**supporting Figure 1**).** Age matched wt mice and IL17ra$^{-/-}$ mice (♂ C57BL/6, 12 w old, n=7/group, 2 independent experiments) were subjected to acute ASH, or pair-fed [24] (see Suppl. text). Mice were sacrificed 9 h after the alcohol-binge treatment. Livers were analyzed by qRT-PCR. (**A**) Serum level of ALT (U/I), body and liver weight, (**B**) expression of fibrogenic genes (Col1a1, αSMA, TIMP1) and inflammatory genes (IL-6, IL-1β, TNF-α) was not changed between wt and IL17ARA$^{-/-}$ mice. The data are the means ± SEM, ns – non specific. Student's *t*-test, *p < 0.05 and **p < 0.01.

Suppl. Figure 2. Chronic alcoholic steatohepatitis is reduced in IL17Ara$^{-/-}$ mice **(**supporting Figure 1). Development of chronic ASH was compared in wt mice and IL17Ara$^{-/-}$ mice (♂ C57BL/6, 12 w old, n=8-10/group, 2 independent experiments). Age-matched litternates were pair-fed or chow-fed (see Suppl. text). (**A**) Serum levels of ALT and AST, blood alcohol, liver and liver/body weight were measured for each group of mice; the gross liver images are shown for wt and IL17Ara$^{-/-}$ mice with chronic alcoholic steatohepatitis. (**B**) Livers were stained with H&E, Sirius Red, and immunostained for F4/80, α-SMA, Desmin, Ly6G, 4-HNE (lipid peroxidation), positive area was calculated as percent. Representative images are taken using x 10, and x 20 objectives. (**C**) Glutathione S-transferase **(**GST**)** and **(D)** Thiobarbituric Acid Reactive Substances (TBARS) were measured to access lipid peroxidation. (**E**) mRNA expression of lipogenic genes, (**F**) ROS production (**G**) neutrophil and macrophage-specific markers and

chemokines, (**H**) inflammatory cytokines, and (**I**) fibrogenic genes were measured using qRT-PCR. One way ANOVA, *p < 0.05 and **p < 0.01.

Suppl. Figure 3. Alcoholic liver fibrosis is reduced in IL17Ara$^{-/-}$ mice (supporting Figure 2**).** Development of alcohol-induced liver fibrosis was induced in IG alcohol-fed wt mice and IL17ra$^{-/-}$ mice (♂ C57BL/6, 12 w old, n=10/group, 2 independent experiments), and compared to pair-fed or chow-fed littermates. (**A**) Serum levels of AST, liver and liver/body weight were measured for each group of mice; the gross liver images are shown for IG alcohol-fed wt and IL17ra$^{-/-}$ mice (see Suppl. text). (**B**) Steatosis (H&E, triglycerides), liver fibrosis (Sirius Red), the number of activated α-SMA^{+} and Desmin^{+} HSCs, Ly6G^{+} neutrophils and F4/80^{+} Kupffer cells, lipid peroxidation (4-HNE) were analyzed by immunostaining and quantified. The data are percent of positive area. Representative images (x 10, x 20 objectives). (**C**) Glutathione S-transferase **(**GST**)** and **(D)** Thiobarbituric Acid Reactive Substances (TBARS) were measured to access lipid peroxidation. (**E**) mRNA expression of lipogenic genes, (**F**) ROS production (**G**) macrophage and neutrophil-specific markers and chemokines, (**H**) inflammatory cytokines, and were measured using qRT-PCR in wt and alcohol-fed IL17ra$^{-/-}$. (**I**) Intracellular expression of IL-17A, IFN-γ, IL-22, and IL-4 cytokines was analyzed in hepatic TCRβ^{+}CD4^{+} (αGal/Cer/mCD1d tetramer^{-}) cells using flow cytometry of the non-parenchymal fraction from IG alcohol-fed mice (EtOH, n=4) vs pair-fed mice (n=5). Representative dot plots are shown, and a summary of the data is presented as bar graphs, mean ± SEM. *p< 0.033, **p<0.0025. One way ANOVA, *p< 0.05 and **p < 0.01.

Suppl. Figure 4. Blockade of IL17A reduces alcoholic liver fibrosis by ≈50% **(**supporting Figure 3**).** (**A**) Outline of the experiment: IG alcohol-fed wt mice (♂ C57BL/6, 12 w old, n=12/group/treatment, 3 independent experiments) were treated (10 after induction of liver injury) with RORγt inhibitor (50 mg/kg/weight vs vehicle, oral gavage 4 x week, or vehicle), or IL17A neutralizing Ab (25 mg/kg/weight vs IgG, i.p. once x week). Serum AST, liver weight was measured in each group of mice. (**B**) Serum levels of IL-6, IL-1β, TNF-α, and IL-10 were measured using ELISA (pg/ml). (**C**) Western blot analysis detected downregulation of IL17A protein in the whole liver lysate from mice treated with RORγt inhibitor (vs IgG). (**D**) qRT-PCR of whole livers from IG alcohol-fed wt mice ± treament. mRNA expression of IL17A was suppressed in RORγt inhibitor-treated mice, but not in mice treated with anti-IL17A neutralizing Ab. (**E**) Livers IG alcohol-fed wt mice ± IL17A Ab (or RORγt inhibitor, not shown) were immunostained for α-SMA, Desmin, Ly6G, F4/80, positive areas were calculated as percent. Representative images (x 10, and x 20 objectives). (**F-G**) qRT-PCR of whole livers from IG alcohol-fed wt mice ± treatment. (**F**) mRNA expression of lipogenic genes, and macrophage-specific markers F4/80 and CD68, and IL-22, (**G**) ROS production were measured using qRT-PCR in IG alcohol-fed wt mice ± RORγt inhibitor (or ± IL17A Ab). Student's *t*-test, *p<0.05, **p<0.01.

Suppl. Figure 5. Blockade of IL17A suppresses hepatic steatosis and activation of Kuppfer cells in IG alcohol-fed mice (supporting Figure 2). Primary hepatocytes and Kupffer cells were isolated from IG alcohol-fed mice ± anti-IL17A Ab using gradient centrifugation method, subjected to RNA-seq analysis, and analyzed by GO terms. The

effect of *in vivo* IL17A blockade on the gene expression profile of hepatocytes and Kupffer cells was evaluated. **(A)** GO terms: the genes upregulated in hepatocytes from IgG- (vs anti-IL17A Ab-) treated mice. **(B)** GO terms: the genes upregulated in hepatocytes from anti-IL17A Ab- (vs IgG-) treated mice. **(C)** RNA-Seq-based expression of selected genes/pathways in hepatocytes and Kupffer cells are shown. **(D)** GO terms: the genes upregulated in Kupffer cells from IgG (vs anti-IL17A Ab-) treated mice. **(E)** GO terms: the genes upregulated in Kupffer cells from anti-IL17A Ab (vs IgG-) treated IG alcohol-fed mice. Significance of the GO terms were indicated as –log 10 (P).

Suppl. Figure 6. Blockage of IL17A ameliorates liver fibrosis in IG alcohol-fed mice, but does not restore microbiome composition in these mice (supporting Figure 3). At least two fesses from IG alcohol fed (or pair-fed) or alcohol-dependent (CIE), or non-dependent, Air) mice were collected. Principal coordinate analysis (PCoA) plots using 16S rRNA visualize the relatedness between gut microbial communities over three experiments. Comparison of the plots for IG alcohol-fed mice (vs pair-fed mice) demonstrates preservation of the gut microbiome in IL17ra$^{-/-}$ mice, despite being fed with IG alcohol. However, gut communities are not restored following the blockade of IL17 signaling (using RORγt inhibitor). Operational taxonomic unit bar plots illustrate the microbial composition at the phylum level for samples collected across three experiments: **(A)** IG-alcohol fed wt mice vs IL17Ara$^{-/-}$mice with alcoholic liver fibrosis, **(B)** IG-alcohol fed wt mice treated with vehicle or Rorγt inhibitor. student's test, *$p<0.01$, **$p<0.05$.

Suppl. Figure 7. IL17A facilitates proliferation/activation of astrocytes and microglia *in vitro* (supporting Figure 4). **(A)** Primary $GFAP^{+}F4/80^{-}$ astrocytes and $GFAP^{-}F4/80^{+}$ microglial cells were isolated from the brains of wt GFAP-GFP reporter mice, and phenotyped by immunocytochemistry. Cell purity was calculated as percent of total cells (representative images x 20 objective). Cultured astrocytes (5 x 10^5 cells, *Astro*) and microglial cells (5 x 10^5 cells, *Micro*) were serum starved (for 18 h), stimulated with IL17A (5ng/ml, for 6 h), expression of selected genes was analyzed using qRT-PCR. The data are average of two independent experiments (triplicates per condition). **(B-D)** Cultured astrocytes (5 x 10^5 cells) were stimulated with TGF-β1 (5ng/ml), or IL-1β (5ng/ml), or vehicle (PBS), and subjected to the customized gene expression microarray[25] (Agilent, see Suppl. text). **(B)** GO terms: for IL-1β- and **(C)** TGF-β- (vs PBS-) stimulated astrocytes are shown. **(D)** Microarray-based expression of selected pro-inflammatory, pro-fibrogenic, and glutamate receptor genes are shown. Student's *t*-test, *p<0.05, **p<0.01. Significance of the GO terms were indicated as –log 10 (P).

Suppl. Figure 8. Blockade of IL17A reduces alcohol-induced brain injury and neuroinflammation (supporting Figure 4)**.** Brains were collected from IG alcohol-fed mice ± RORγt inhibitor, or anti-IL17A Ab, and immunostained for Iba1 and DAPI to visualize microglia. **(A)** The number of $Iba1^{+}DAPI^{+}$ cells in hippocampus was calculated as percent of all $DAPI^{+}$ cells. **(B)** The $Iba1^{+}$ positive area in hippocampus was calculated as percent. **(C)** mRNA expression of IL17RA, and IL-1β were measured in the whole brains from chow-fed, pair-fed, and IG alcohol-fed mice ± anti-IL17A Ab mice using

qRT-PCR. **(D)** Coronal brain sections were immunostained for active Caspase 3 to visualize apoptotic neurons. Caspase 3^+ staining was detected in the cerebellum of IG alcohol-fed mice ± anti-IL17A Ab along the neuronal axons. Caspase 3 expression was markedly reduced in cerebellum of IG alcohol-fed mice treated with anti-IL17A Ab. Caspase 3^+ positive area was calculated as percent, representative images were taken using x 20 and x 100 objectives. **(E)** Frontal cortex, cerebellum, and hippocampus were microdissected from the brains of IG alcohol-fed mice ± anti-IL17A Ab, expression of GFAP mRNA was measured using qRT-PCR. One way ANOVA, *$p < 0.05$ and **$p < 0.01$.

Suppl. Figure 9. IG alcohol-induced brain injury is associated with development of neuroinflammation (supporting Figure 4**).** **(A)** Expression of IL17A and IL17RA mRNA was compared in the brains, livers, and lungs isolated from the IG alcohol-fed wt mice (vs chow- and pair-fed wt mice). IL17A mRNA was induced in the livers but not in the brains, or lungs of IG alcohol-fed wt mice (the data are relative mRNA expression level). IL17RA mRNA was induced in livers, brains, and lungs of IG alcohol-fed mice. **(B)** Cortex, hippocampus, and cerebellum were microdissected from the brains of IG alcohol-fed wt mice (vs chow-, and pair-fed wt mice, n=3-4 per group) and analyzed by qRT-PCR. Upregulation of IL17RA mRNA was detected in the brains of IG alcohol-fed mice, especially in the hippocampus (↑1.7 fold vs chow-fed mice). **(C)** Coronal brain sections were analyzed by RNA *in situ* hybridization for expression of IL17A mRNA in IG alcohol-fed mice. IL17A mRNA signal was observed in the livers but not in the brains (isolated from the same IG alcohol-fed wt mice). **(D)** Cerebrospinal fluid (CSF) was

isolated from IG-alcohol-fed wt mice (vs chow-, and pair-fed wt mice, n=7-10 per group) and analyzed for the presence of IL17A and other inflammatory cytokines using ELISA. IL17A cytokine was detected in CSF of IG-alcohol-fed mice (↑ 6 fold vs pair-fed). The CSF levels of other pro-inflammatory cytokines (↑ 2 fold IL-1β, ↑ 2 fold TGF-β1, and ↑ 1.3 fold TNF-α), that are indicative of alcohol-induced neuroinflammation, were also increased in these mice. Student's *t*-test, *p<0.05, **p<0.01.

Suppl. Figure 10. Development of neuroinflammation in IG alcohol-fed mice is associated with increased BBB permeability (supporting Figure 4**).** **(A)** The presence of albumin CSF was tested in the CSF of IG alcohol-fed mice ± RORγt inhibitor (vs vehicle-treated, or pair-fed mice) using ELISA, the data are pg/ml. **(B-C)** Brains from IG alcohol-fed ± RORγt inhibitor (or vehicle), and pair-fed mice were co-stained for Zo-1 (tight junction protein expressed by endothelial cells) and albumin (serum marker which does not cross BBB under physiological conditions). **(B)** Positive area of extravazated albumin (red) was quantified as percent. **(C)**. Representative images were taken using x 4, x 40 objectives. Immunoreactivity for albumin in the pair-fed mice was constrained to the blood vessels (yellow arrows). Extravasation of albumin into the brain parenchyma (white arrows) was observed only in IG alcohol-fed mice. Blocking of IL17A signaling did not reduce albumin content in IG alcohol-fed mice ± RORγt inhibitor, indicating that BBB permeability in these mice is caused by alcohol (rather than Th17 cells). Student's *t*-test, *p<0.05, **p<0.01, ns – non-specific.

Suppl. Figure 11. IL17A facilitates astrocyte activation in alcohol-dependent mice (supporting Figure 5 and 6). Mice (♂ C57BL/6, n=10/group, 2 independent experiments) developed alcohol dependence (CIE) vs non-dependent controls (Air), and treated with ± anti-IL17A Ab (vs IgG). **(A)** Serum cytokines (IL17A, TNF-α and IL-1β,) were measured using ELISA in naïve mice, in alcohol-dependent (after CIE) in non-dependent mice (after Air) mice, and 24hr after 2BC sessions. The data are pg/ml, (triplicates, 2 independent experiments). **(B-C)** (supporting Figure 5). Coronal brain sections from Air and CIE mice ± anti-IL17A Ab were co-stained for GFAP. **(C)** Representative images of the frontal cortex are shown (x 40, x 60 objectives). **(C)** Representative images of the Hippocampus (nucleai are visualized by DAPI, astrocytes are visualized by co-staining for GFAP and Sox9) are shown (x 100 objective). **(E)** GFAP positive area in the cortex or Hippocampus area was calculated as percent. The number of $GFAP^{+}Sox9^{+}$ astrocytes in Hippocampus was calculated as percent (vs Air + IgG mice), Student's *t*-test, *p<0.05, **p<0.01.

Suppl. Figure 12. IL17A is increased in serum of alcohol-dependent mice (supporting Figure 7**).** Naïve co-housed mice (♂ C57BL/6, n=6/group, 4 independent experiments) developed alcohol dependence (CIE) vs non-dependent controls (Air) and subjected to sessions of volunteer alcohol drinking (2BC). **(A)** Livers were isolated from Air and CIE mice and analyzed for steatosis (Oil Red O), and liver fibrosis (Sirius Red). Livers were stained for Desmin and F4/80 to visualize Hepatic Stellate Cells (HSCs) and Kupffer cells, respectively. Representative images (x 20 objective). The positive area was calculated as percent. **(B)** Coronal brain sections were analyzed using *in situ*

hybridization for expression of IL17A mRNA in CIE mice. IL17A mRNA signal was not observed in the cortex or Hippocampus of CIE mice. Representative images (x 10, and x 40 objectives). **(C)** The whole lungs and livers were analyzed using qRT-PCR. Strong induction of IL17A mRNA expression was detected in the lungs of CIE (vs Air) mice. **(D)** Expression of fibrogenic and inflammatory genes were analyzed in the whole lungs from CIE vs Air mice. Exposure to the EtOH vapor did not induce lung fibrosis in CIE mice. **(E)** Analysis of BBB permeability: Evans blue dye was injected i.v. into the mice 30 min prior to sacrifice. Brains were perfused, Evans blue dye was extracted from the brains, and quantified using spectrophotometric analysis, the data are mg/g brain tissue. **(F)** Expression of IL17RA and pro-inflammatory cytokines was measured in the whole brains using qRT-PCR. **(G)** Cerebrospinal fluid (CSF) was isolated from naïve, alcohol-dependent (after CIE), and non-dependent mice (after Air) mice and after 2BC sessions. The data are pg/ml (triplicates, 2 independent experiments). IL17A cytokine or serum albumin were not detected in CSF of CIE or AIR mice. Student's *t*-test *p<0.05, **p<0.01.

Suppl. Figure 13. Development of alcohol-depencence in CIE mice is associated with dysregulation of astrocyte activation in the hippocampus of alcohol-dependent mice (supporting Figure 8 and 9**).** Similar to previous reports (PMID: 21464311, 24082084, 26730594), differential expression analysis identified alcohol-dependence associated hippocampal pathways, which were dysregylated in CIE mice + IgG (compared to Air mice + IgG), but were restored in CIE mice treated with anti-IL17A Ab (determined

using GSEA). Heatmaps demonstrating the pathways of alcohol-dependence associated hippocampal genes in CIE mice + anti-IL17A Ab vs (+ IgG, $p<0.05$), log fold changes.

Supplemental References:

1. Bertola, A., Mathews, S., Ki, S.H., Wang, H. & Gao, B. Mouse model of chronic and binge ethanol feeding (the NIAAA model). *Nat Protoc* **8**, 627-637 (2013).
2. Page, A.*, et al.* Alcohol directly stimulates epigenetic modifications in hepatic stellate cells. *J Hepatol* **62**, 388-397 (2015).
3. US Department of Health and Human Services. National Institute of Health/National Institute on Alcohol Abuse and Alcoholism. Helping Patients who drink too much. A clinician's guide Updated 2005 Edition. http://pubs.niaaa.nih.gov/publications/Practitioner/CliniciansGuide2005/guide.pdf. (2005).
4. Sobell, L.C. & Sobell, M.B. Timeline follow-back: A technique for assessing self-reported alcohol consumption. in *Measuring alcohol consumption: Psychosocial and biochemical methods* (eds. Litten, R.Z. & Allen, J.P.) 41-72 (Humana Press, Inc, 1992).
5. Sobell, L.C. & Sobell, M.B. *Timeline FollowBack: User's guide*, (Addicition Research Foundation, Toronto, 1996).
6. Wang, F.*, et al.* RNAscope: a novel in situ RNA analysis platform for formalin-fixed, paraffin-embedded tissues. *J Mol Diagn* **14**, 22-29 (2012).
7. Seki, E.*, et al.* TLR4 enhances TGF-beta signaling and hepatic fibrosis. *Nat Med* **13**, 1324-1332 (2007).
8. Dobin, A.*, et al.* STAR: ultrafast universal RNA-seq aligner. *Bioinformatics* **29**, 15-21 (2013).
9. Heinz, S.*, et al.* Simple combinations of lineage-determining transcription factors prime cis-regulatory elements required for macrophage and B cell identities. *Mol Cell* **38**, 576-589 (2010).
10. Robinson, M.D., McCarthy, D.J. & Smyth, G.K. edgeR: a Bioconductor package for differential expression analysis of digital gene expression data. *Bioinformatics* **26**, 139-140 (2010).
11. Kumamaru, H.*, et al.* Liposomal clodronate selectively eliminates microglia from primary astrocyte cultures. *J Neuroinflammation* **9**, 116 (2012).
12. Lee, J.D.*, et al.* Blood-brain barrier dysfunction occurring in mice infected with Angiostrongylus cantonensis. *Acta Trop* **97**, 204-211 (2006).
13. Meng, F.*, et al.* Interleukin-17 signaling in inflammatory, Kupffer cells, and hepatic stellate cells exacerbates liver fibrosis in mice. *Gastroenterology* **143**, 765-776 e761-763 (2012).
14. Radu, M. & Chernoff, J. An in vivo assay to test blood vessel permeability. *J Vis Exp*, e50062 (2013).
15. Caporaso, J.G.*, et al.* Global patterns of 16S rRNA diversity at a depth of millions of sequences per sample. *Proc Natl Acad Sci U S A* **108 Suppl 1**, 4516-4522 (2011).
16. Tsukamoto, H., Mkrtchyan, H. & Dynnyk, A. Intragastric ethanol infusion model in rodents. *Methods Mol Biol* **447**, 33-48 (2008).

17. Xiong, S.*, et al.* Hepatic macrophage iron aggravates experimental alcoholic steatohepatitis. *Am J Physiol Gastrointest Liver Physiol* **295**, G512-521 (2008).
18. Yan, A.W.*, et al.* Enteric dysbiosis associated with a mouse model of alcoholic liver disease. *Hepatology* **53**, 96-105 (2011).
19. Yan, A.W. & Schnabl, B. Bacterial translocation and changes in the intestinal microbiome associated with alcoholic liver disease. *World journal of hepatology* **4**, 110-118 (2012).
20. Acarin, L., Gonzalez, B. & Castellano, B. Neuronal, astroglial and microglial cytokine expression after an excitotoxic lesion in the immature rat brain. *Eur J Neurosci* **12**, 3505-3520 (2000).
21. Semple, B.D.*, et al.* Interleukin-1 Receptor in Seizure Susceptibility after Traumatic Injury to the Pediatric Brain. *J Neurosci* **37**, 7864-7877 (2017).
22. Iwakura, Y., Ishigame, H., Saijo, S. & Nakae, S. Functional specialization of interleukin-17 family members. *Immunity* **34**, 149-162 (2011).
23. Nicoletti, F., Bruno, V., Copani, A., Casabona, G. & Knopfel, T. Metabotropic glutamate receptors: a new target for the therapy of neurodegenerative disorders? *Trends Neurosci* **19**, 267-271 (1996).
24. Ki, S.H.*, et al.* Interleukin-22 treatment ameliorates alcoholic liver injury in a murine model of chronic-binge ethanol feeding: role of signal transducer and activator of transcription 3. *Hepatology* **52**, 1291-1300 (2010).
25. Saijo, K.*, et al.* A Nurr1/CoREST pathway in microglia and astrocytes protects dopaminergic neurons from inflammation-induced death. *Cell* **137**, 47-59 (2009).

Supplemental Figure 1

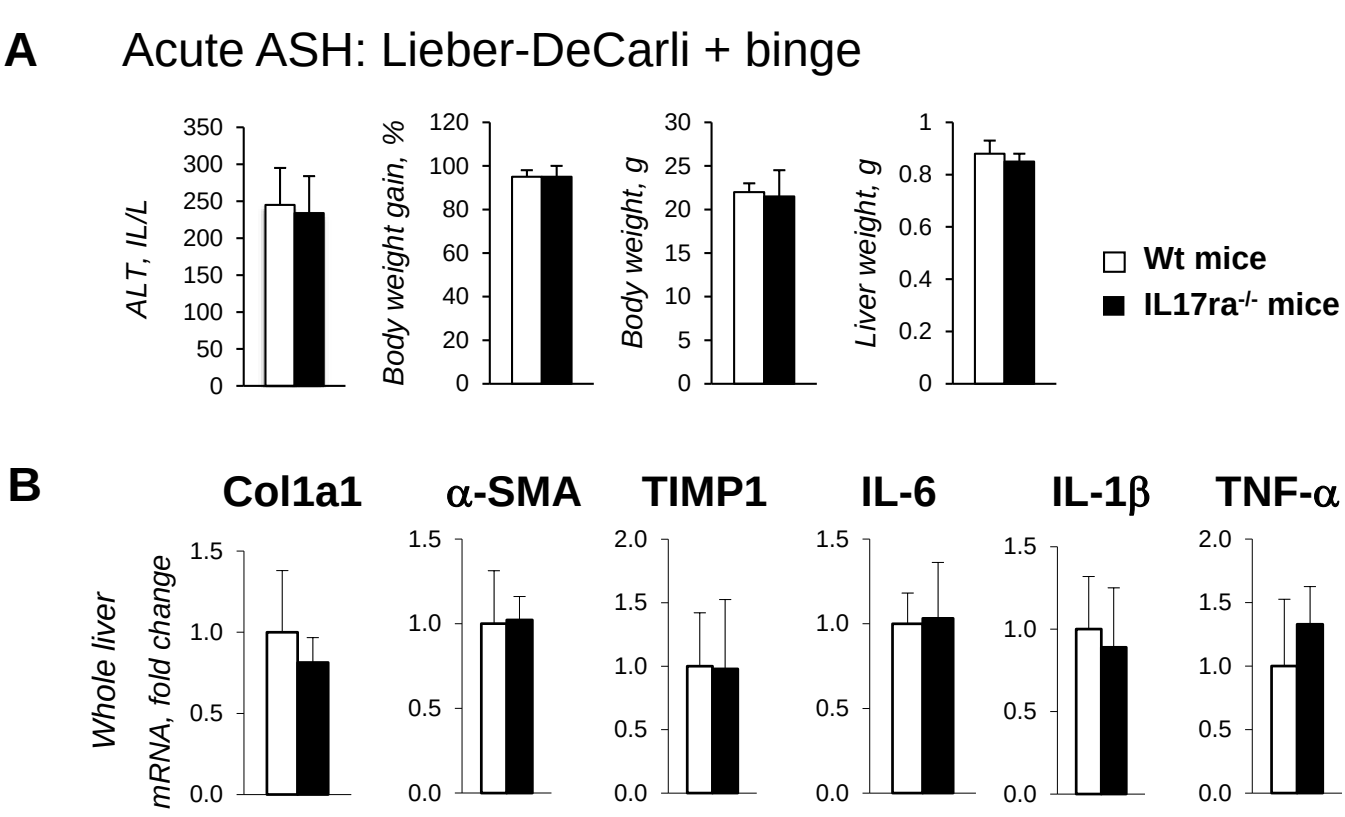

Supplemental Figure 2

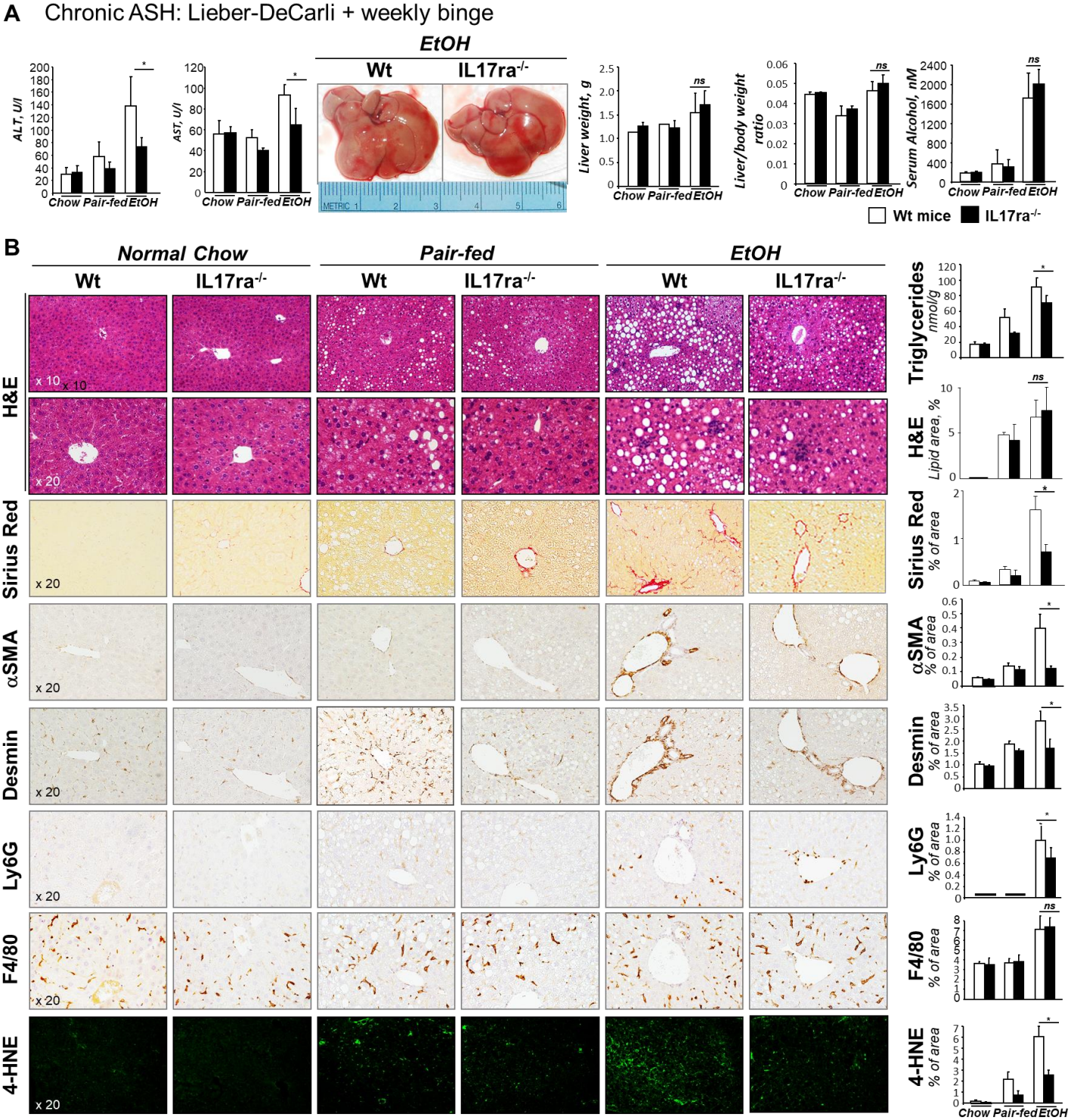

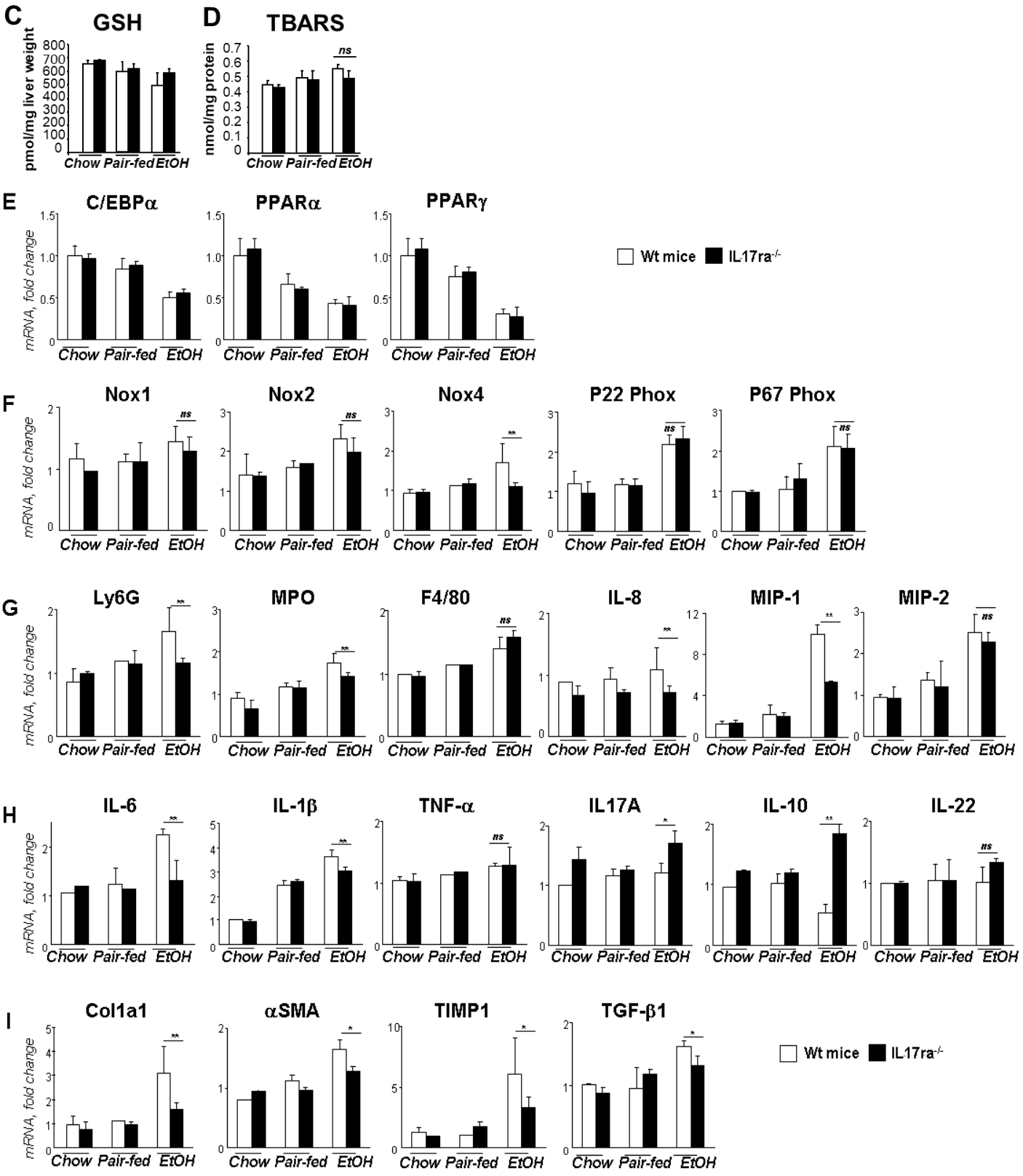
C
GSH
pmol/mg liver weight
800
700
600
500
400
300
200
100
0
Chow Pair-fed EtOH
D
TBARS
nmol/mg protein
0.7
0.6
0.5
0.4
0.3
0.2
0.1
0
ns
Chow Pair-fed EtOH
E
C/EBPα
PPARα
PPARγ
mRNA, fold change
1.5
1.0
0.5
0
Chow Pair-fed EtOH
Wt mice
IL17ra-/-
F
Nox1
Nox2
Nox4
P22 Phox
P67 Phox
mRNA, fold change
ns
**
Chow Pair-fed EtOH
G
Ly6G
MPO
F4/80
IL-8
MIP-1
MIP-2
mRNA, fold change
**
ns
Chow Pair-fed EtOH
H
IL-6
IL-1β
TNF-α
IL17A
IL-10
IL-22
mRNA, fold change
*
**
ns
Chow Pair-fed EtOH
I
Col1a1
αSMA
TIMP1
TGF-β1
mRNA, fold change
*
**
Chow Pair-fed EtOH
Wt mice
IL17ra-/-

Supplemental Figure 3

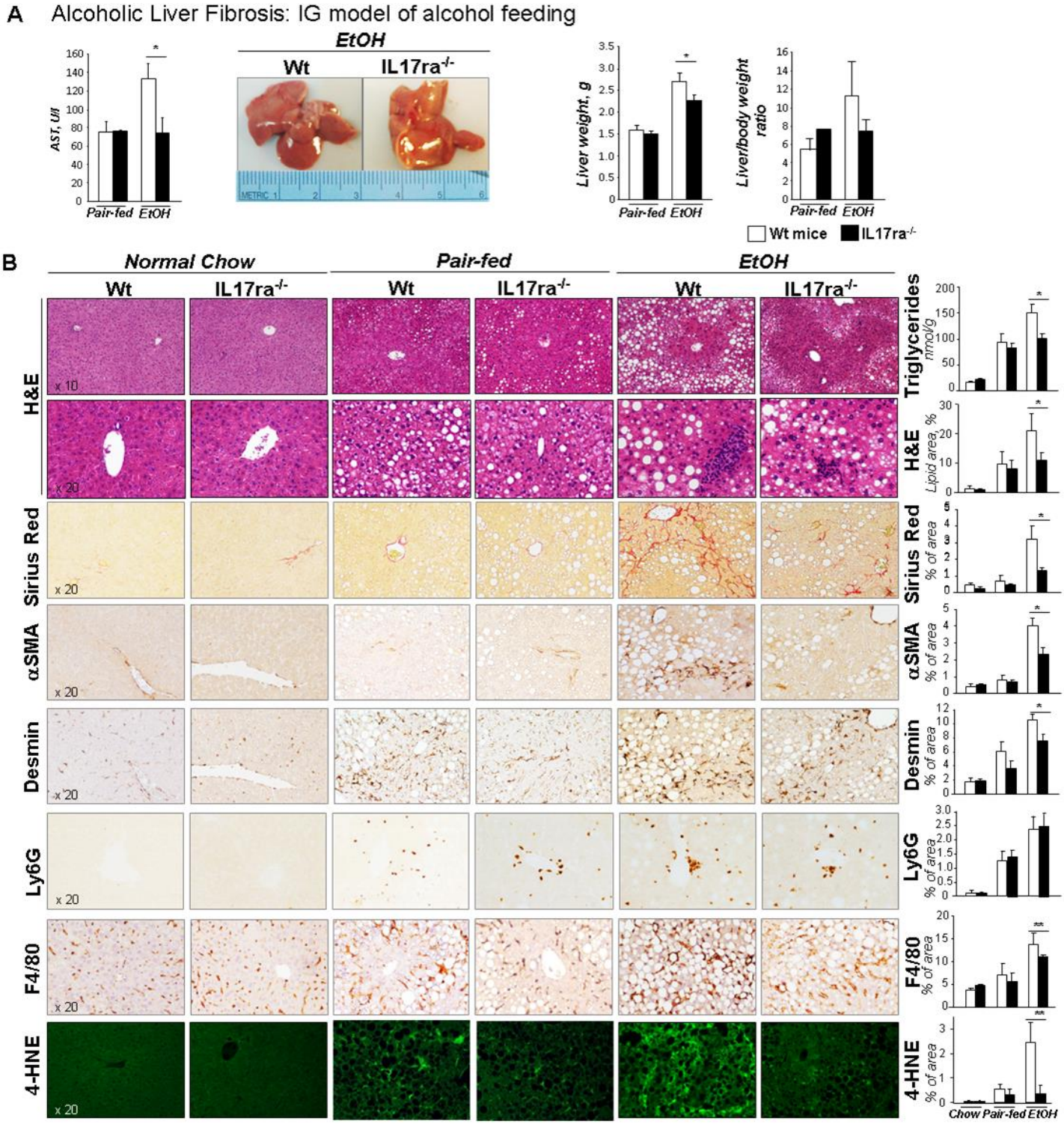

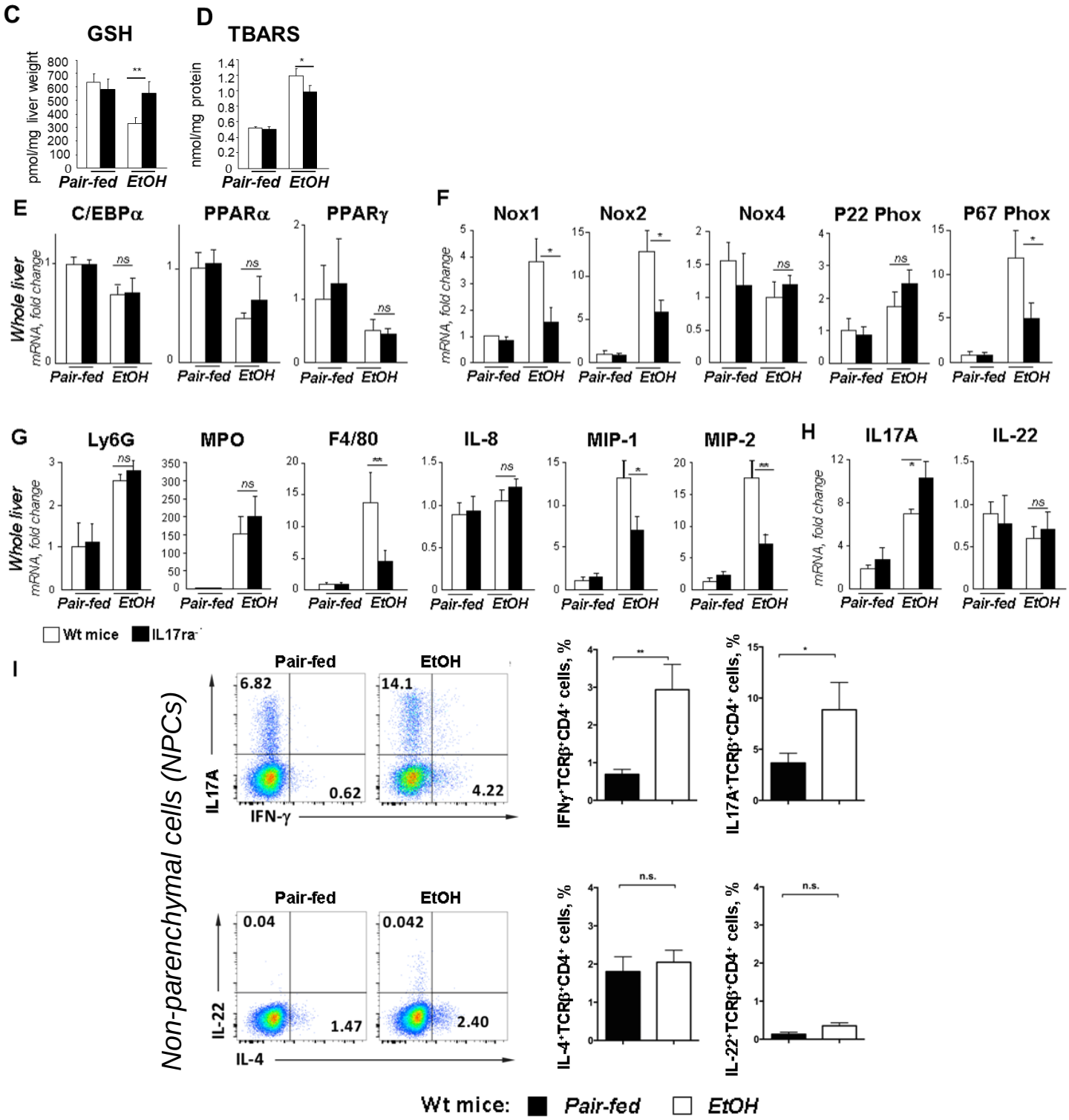
C
GSH
pmol/mg liver weight
Pair-fed
EtOH
D
TBARS
nmol/mg protein
E
C/EBPα
PPARα
PPARγ
Whole liver
mRNA, fold change
ns
F
Nox1
Nox2
Nox4
P22 Phox
P67 Phox
G
Ly6G
MPO
F4/80
IL-8
MIP-1
MIP-2
H
IL17A
IL-22
Wt mice
IL17ra-/-
I
Non-parenchymal cells (NPCs)
6.82
0.62
14.1
4.22
IL17A
IFN-γ
IFNγ+TCRβ+CD4+ cells, %
IL17A+TCRβ+CD4+ cells, %
0.04
1.47
0.042
2.40
IL-22
IL-4
IL-4+TCRβ+CD4+ cells, %
IL-22+TCRβ+CD4+ cells, %
n.s.
Wt mice: Pair-fed EtOH

Supplemental Figure 4

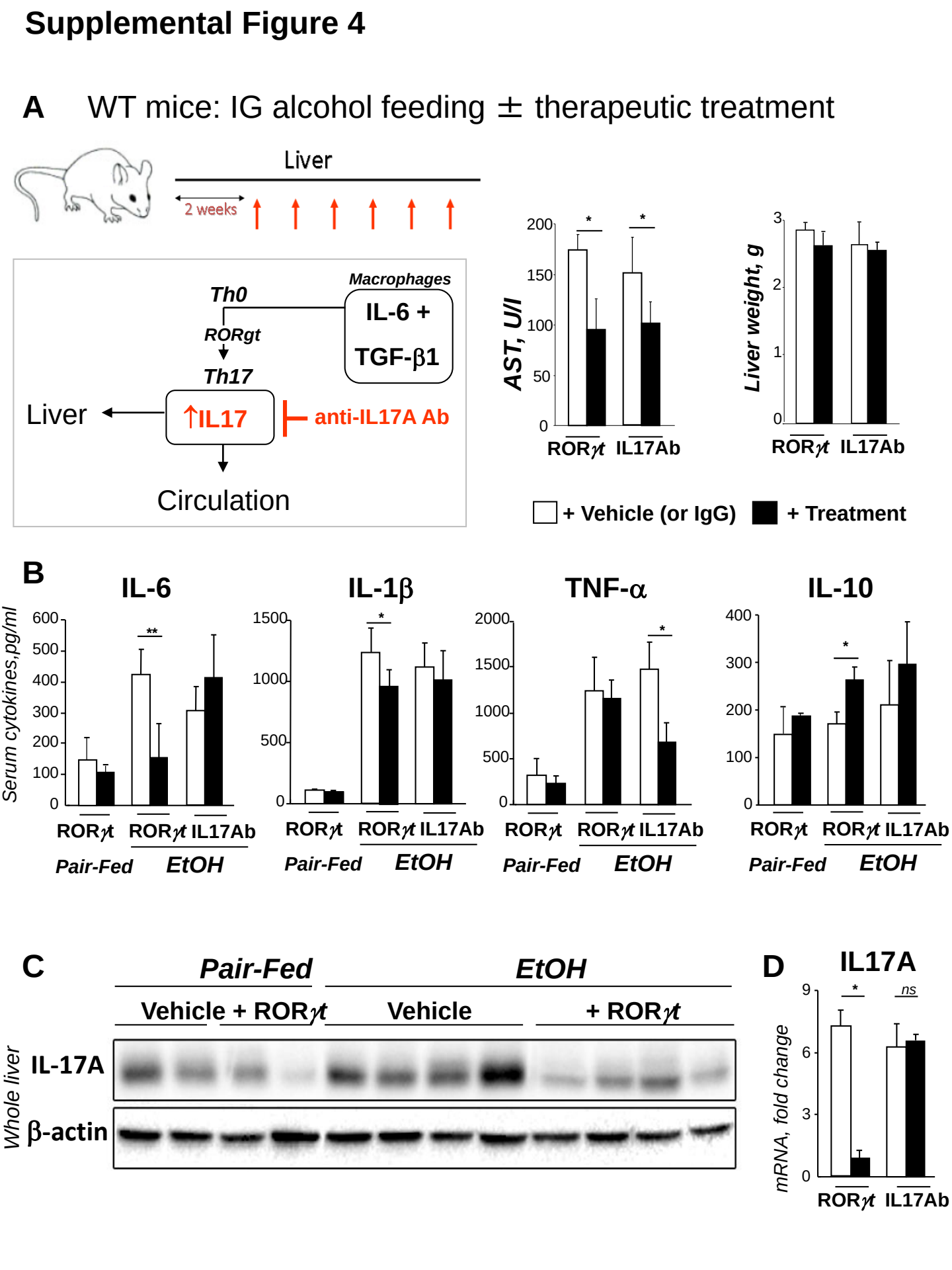

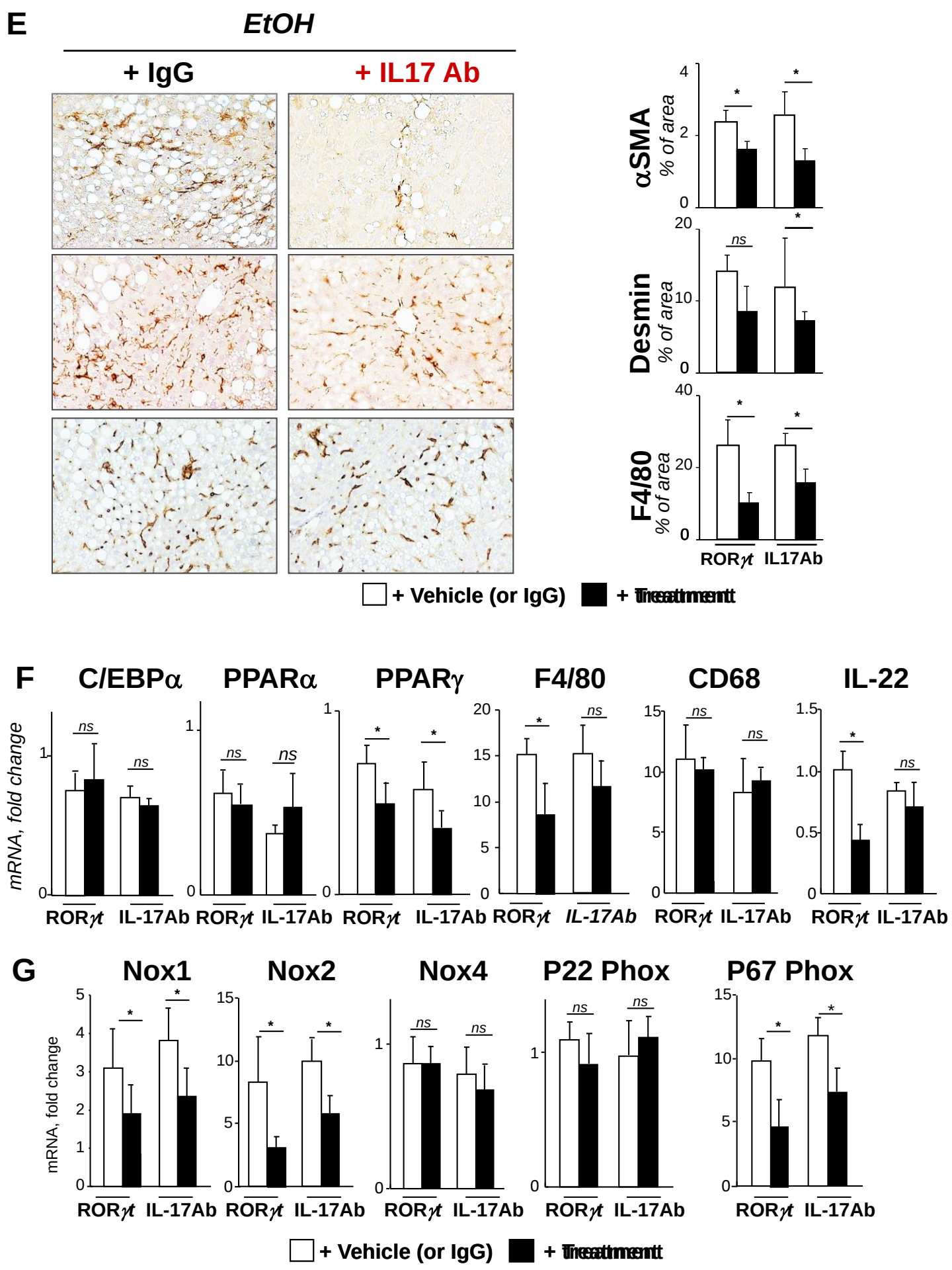
E
EtOH
+ IgG
+ IL17 Ab
αSMA
% of area
Desmin
% of area
F4/80
% of area
RORγt
IL17Ab
+ Vehicle (or IgG)
+ Treatment
F
C/EBPα
PPARα
PPARγ
F4/80
CD68
IL-22
mRNA, fold change
RORγt
IL-17Ab
IL-17Ab
G
Nox1
Nox2
Nox4
P22 Phox
P67 Phox
mRNA, fold change
RORγt
IL-17Ab
+ Vehicle (or IgG)
+ Treatment

Supplemental Figure 5

A IG alcohol fed wt mice ± anti-IL17 Ab (or IgG)

Primary Hepatocytes:
Genes upregulated in IgG- vs anti-IL17 Ab-treated mice:

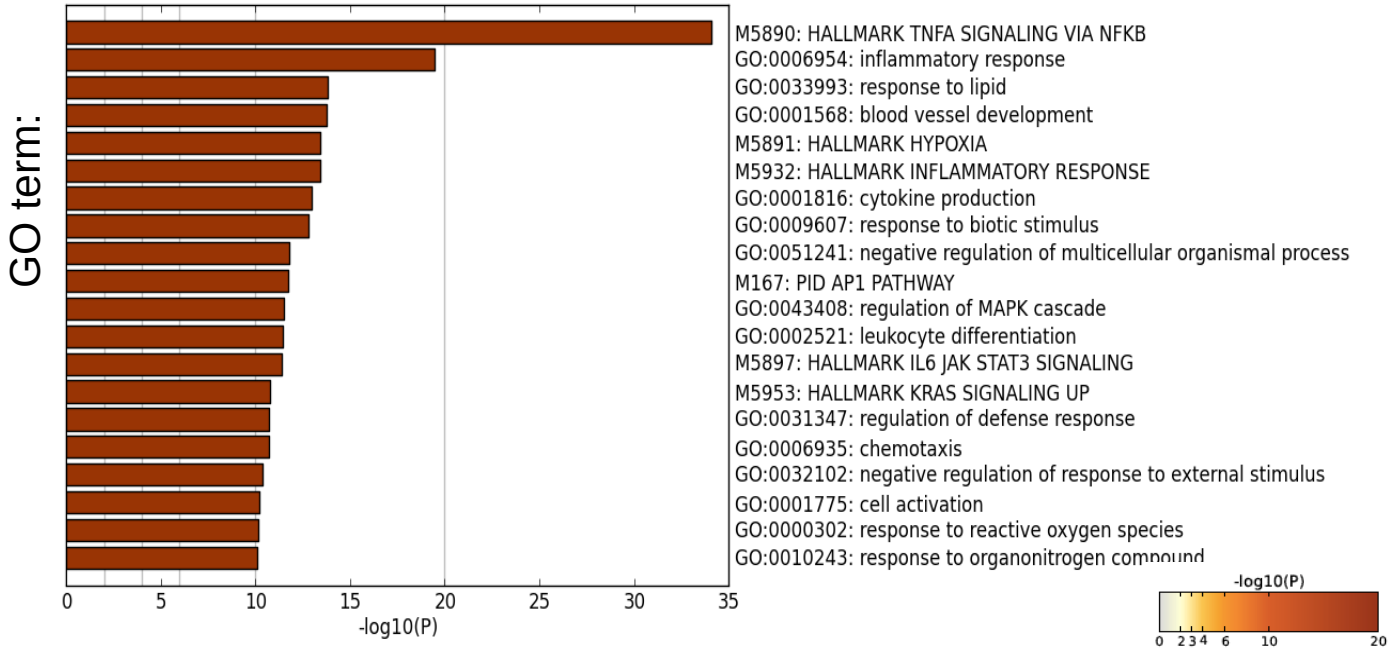

B

Primary Hepatocytes:
Genes upregulated in anti-IL17 Ab- vs IgG-treated mice:

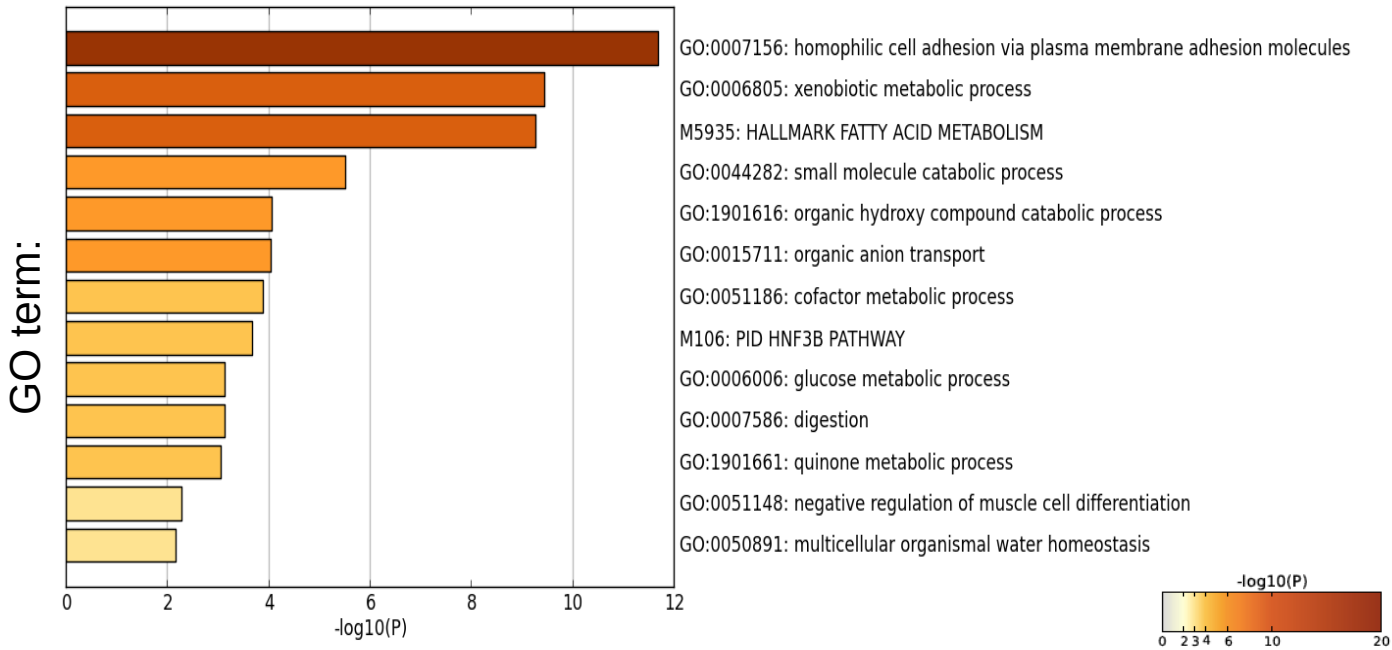

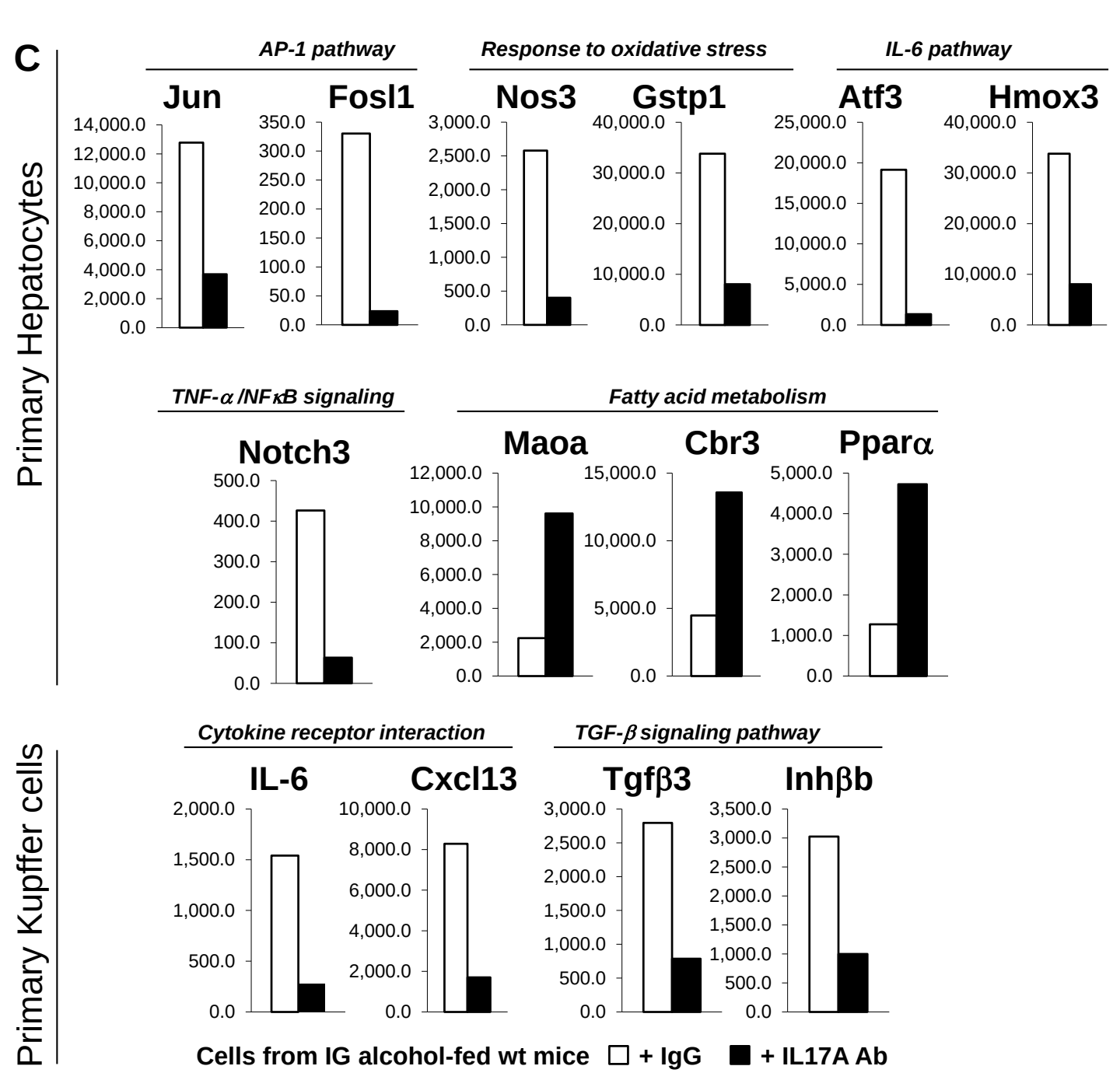
C
Primary Hepatocytes
AP-1 pathway
Response to oxidative stress
IL-6 pathway
Jun
Fosl1
Nos3
Gstp1
Atf3
Hmox3
TNF-α/NFκB signaling
Fatty acid metabolism
Notch3
Maoa
Cbr3
Pparα
Primary Kupffer cells
Cytokine receptor interaction
TGF-β signaling pathway
IL-6
Cxcl13
Tgfβ3
Inhβb
Cells from IG alcohol-fed wt mice
+ IgG
+ IL17A Ab

D

Primary Kupffer cells:
Genes upregulated in IgG- vs anti-IL17A Ab-treated mice:

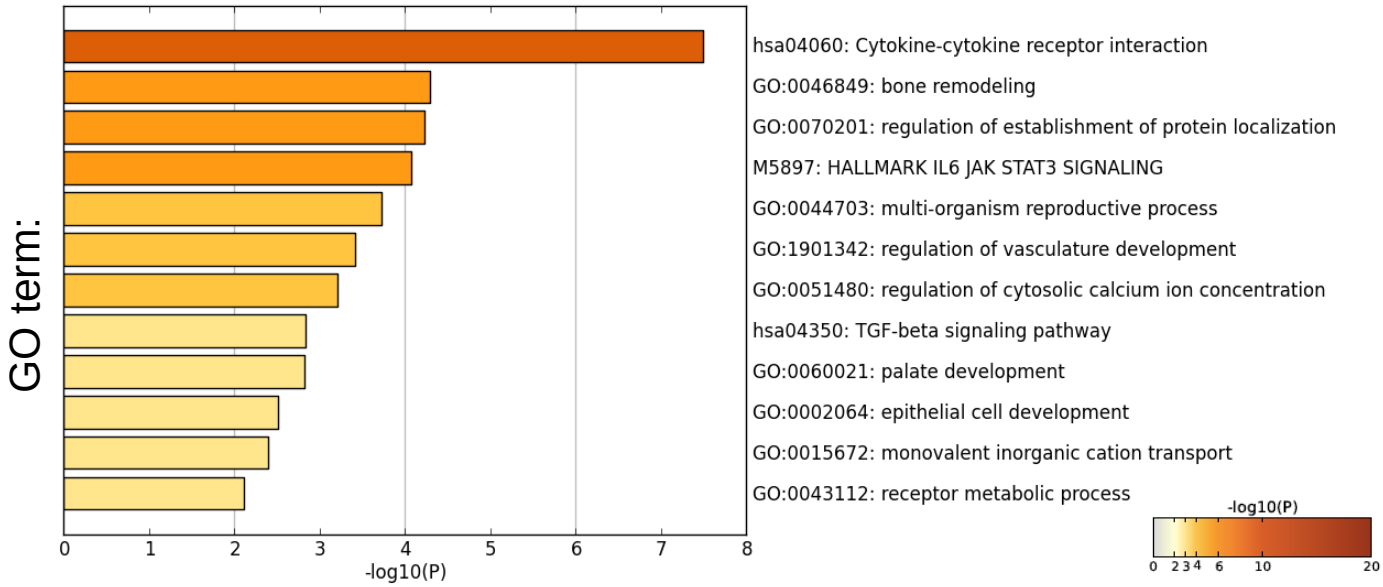

E

Primary Kupffer cells:
Genes upregulated in anti-IL17A Ab- vs IgG-treated mice:

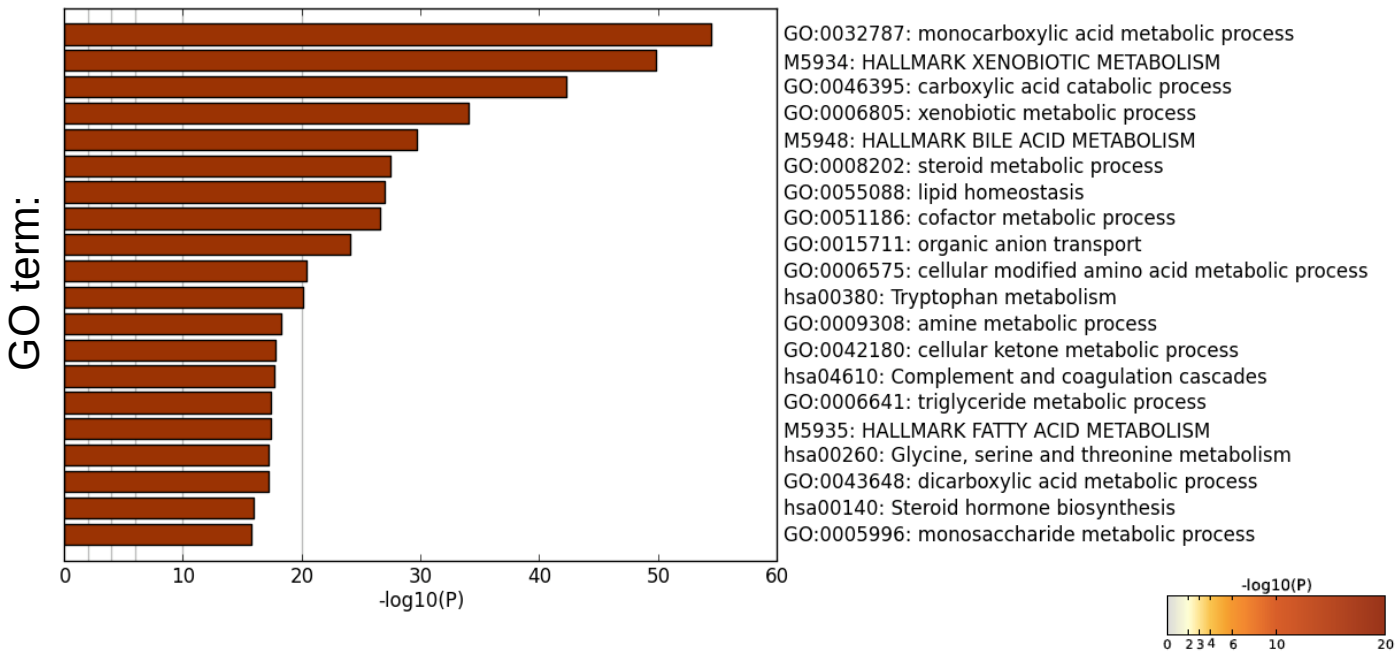

Supplemental Figure 6

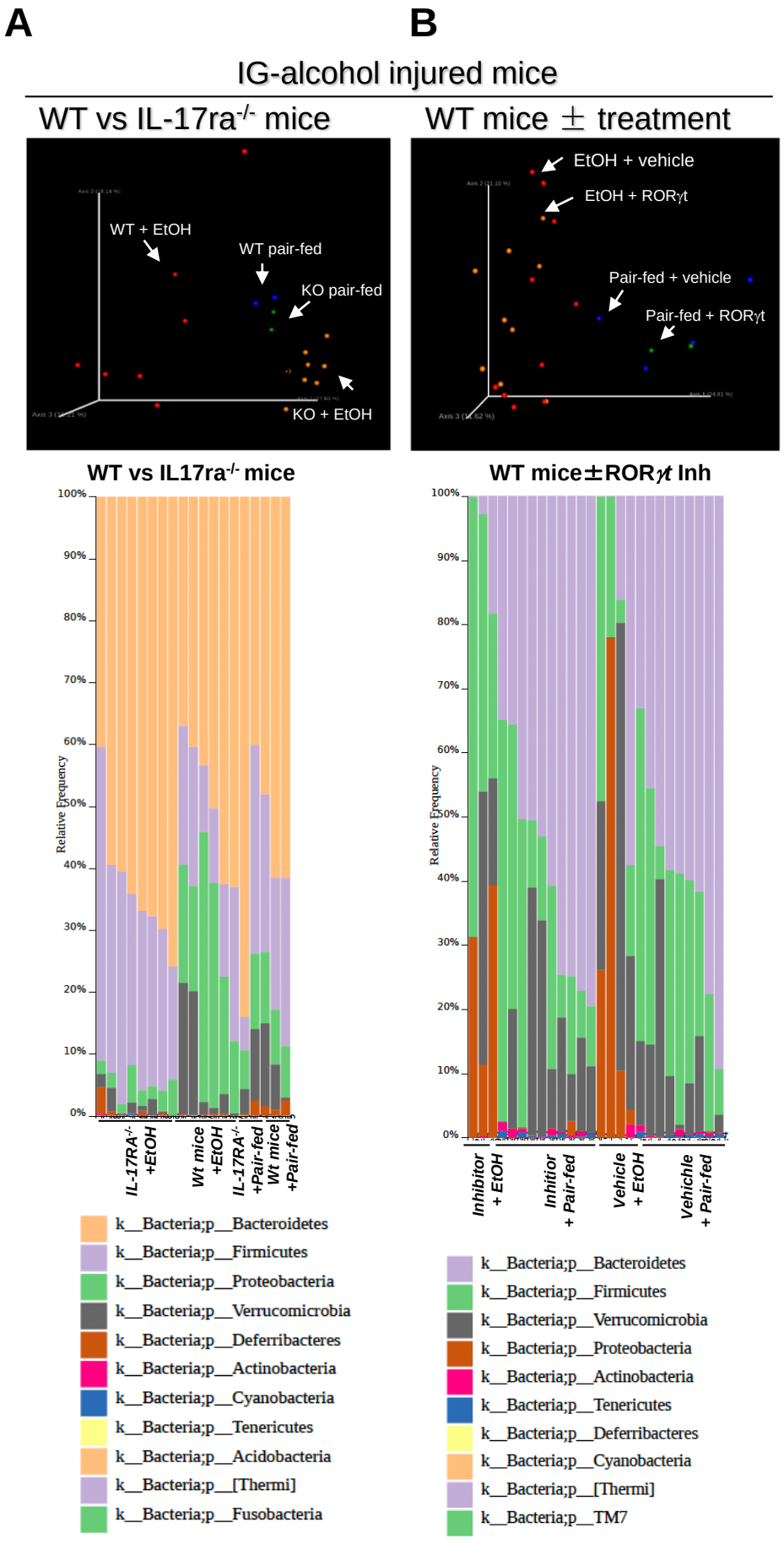

Supplemental Figure 7

A

Cultured primary cells ☐ + Vehicle ■ + IL-17A

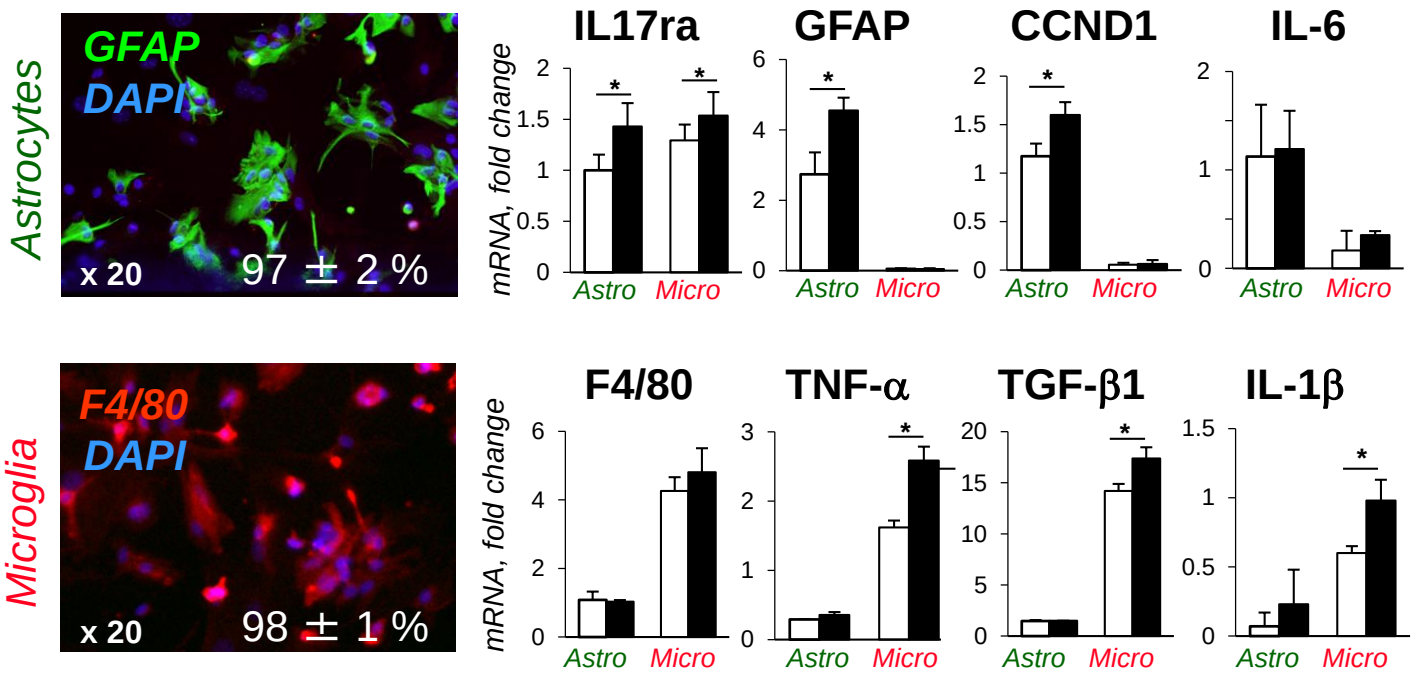

B

Genes upregulated in IL-1β-stimulated vs. PBS astrocytes

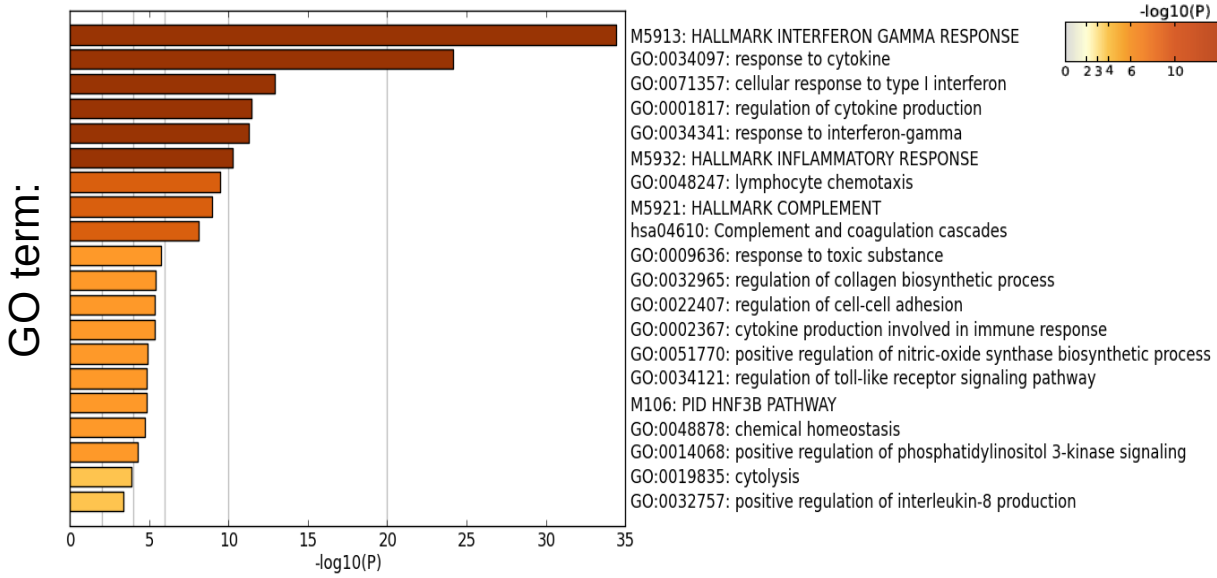

C Genes upregulated in TGF-β1-stimulated vs. PBS astrocytes

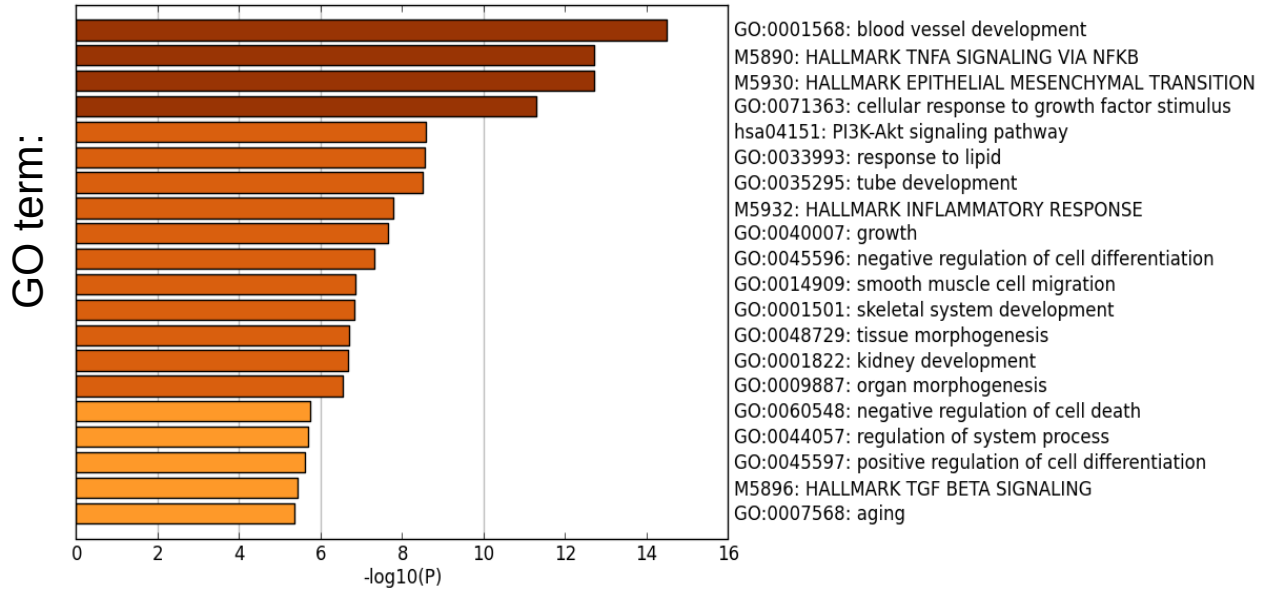

D Cultured primary astrocytes □ + Vehicle ▒ + TGF-β1 ■ + IL-1β

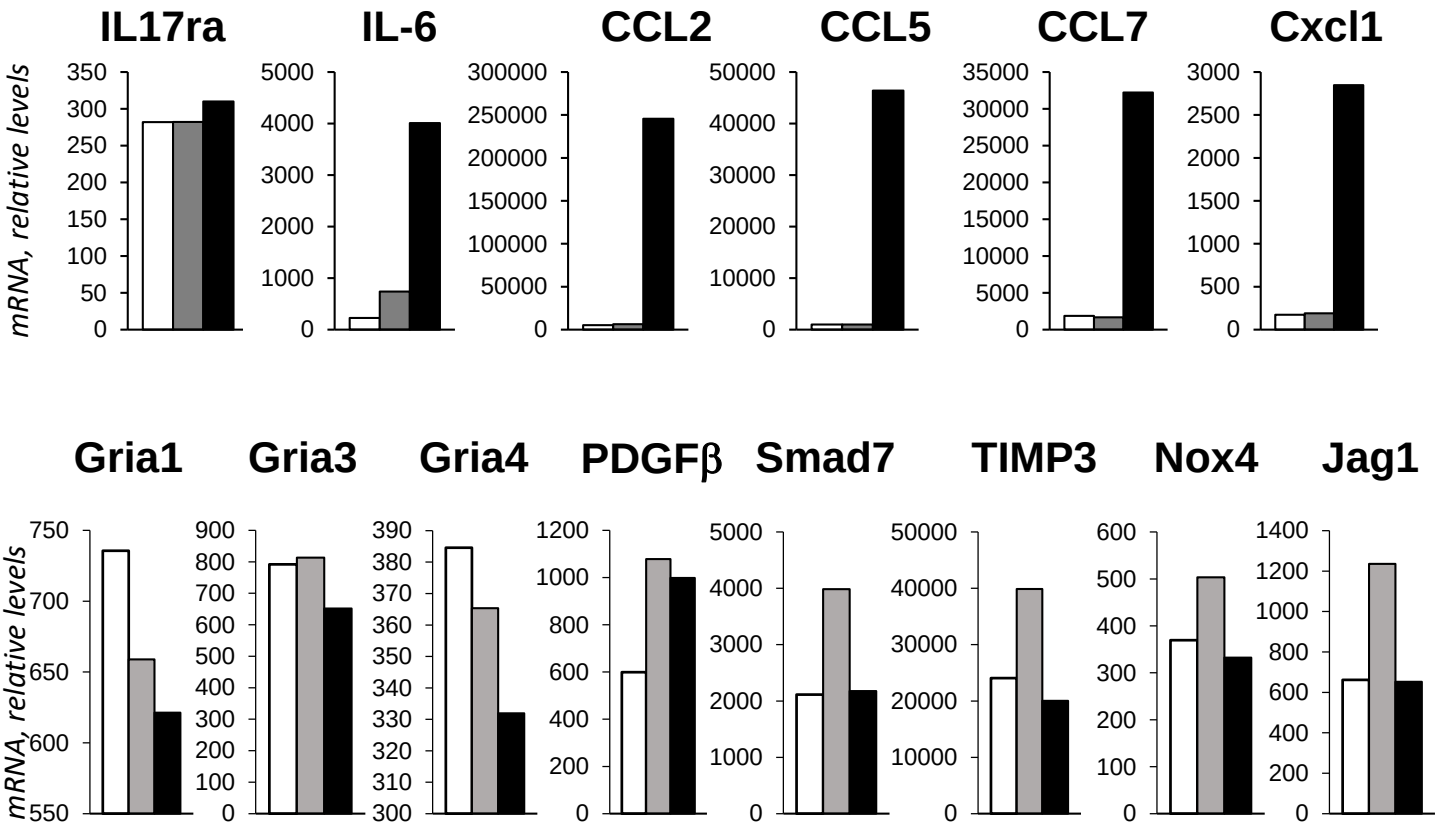

Supplemental Figure 8

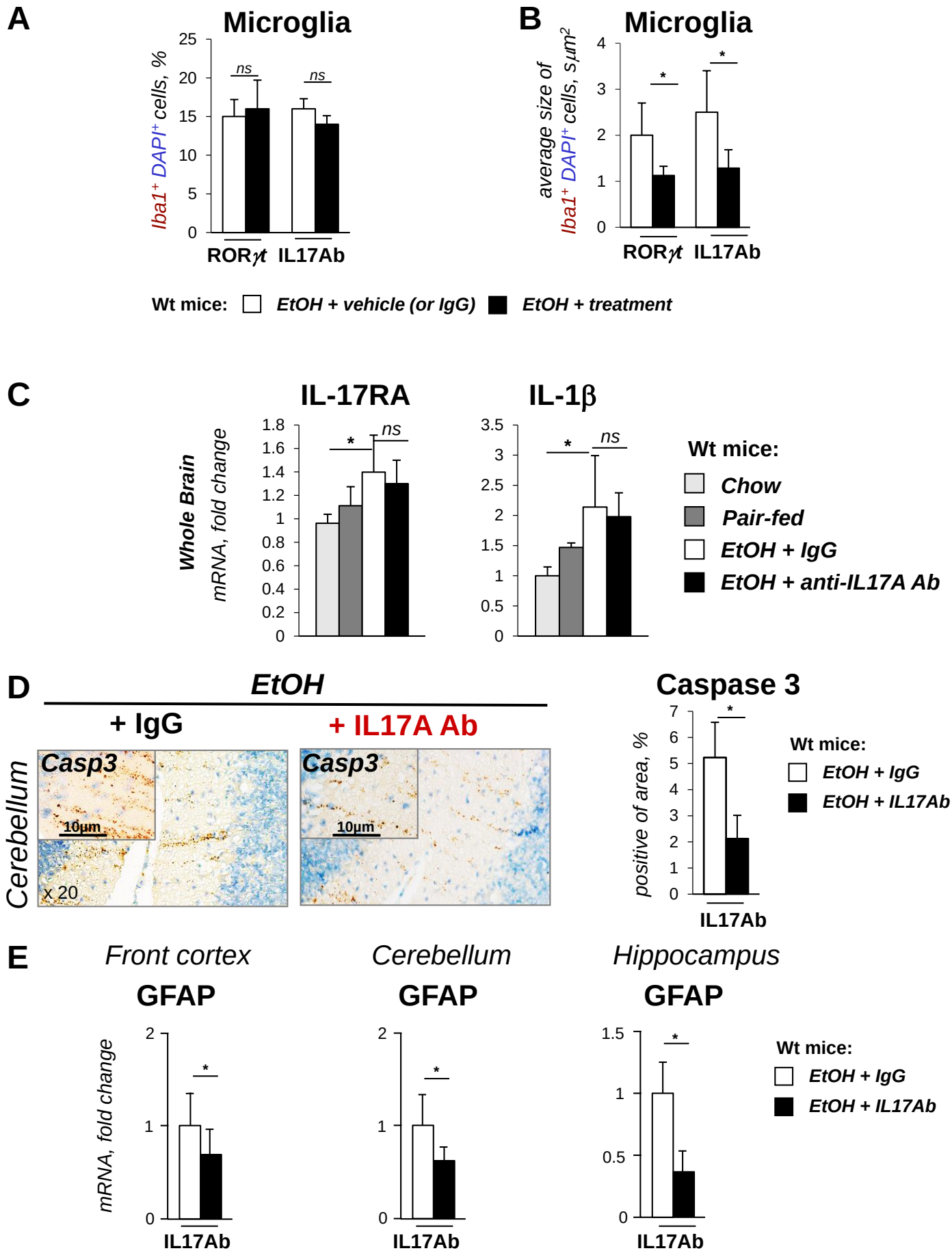

Supplemental figure 9

IG alcohol-fed wt mice:

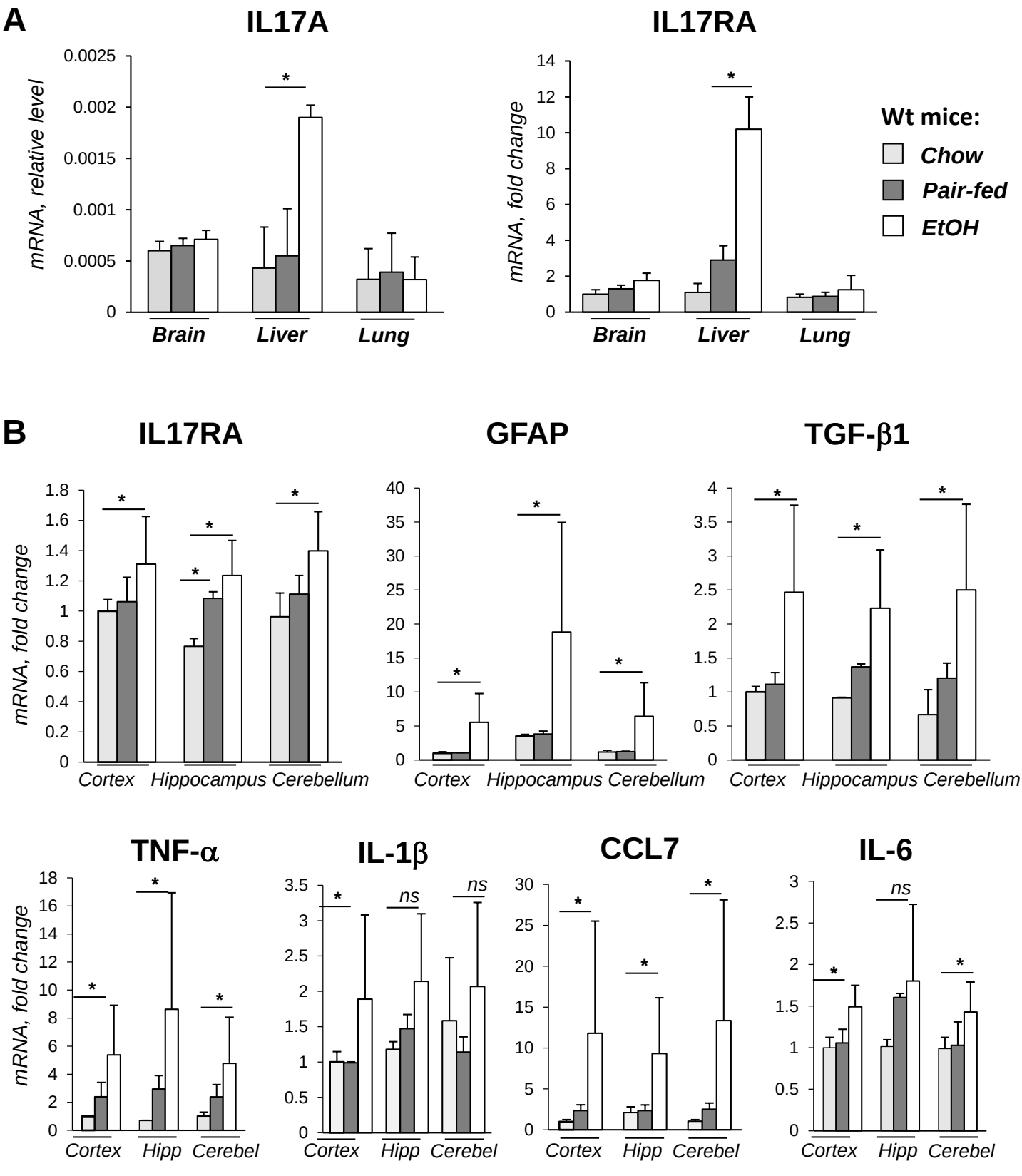

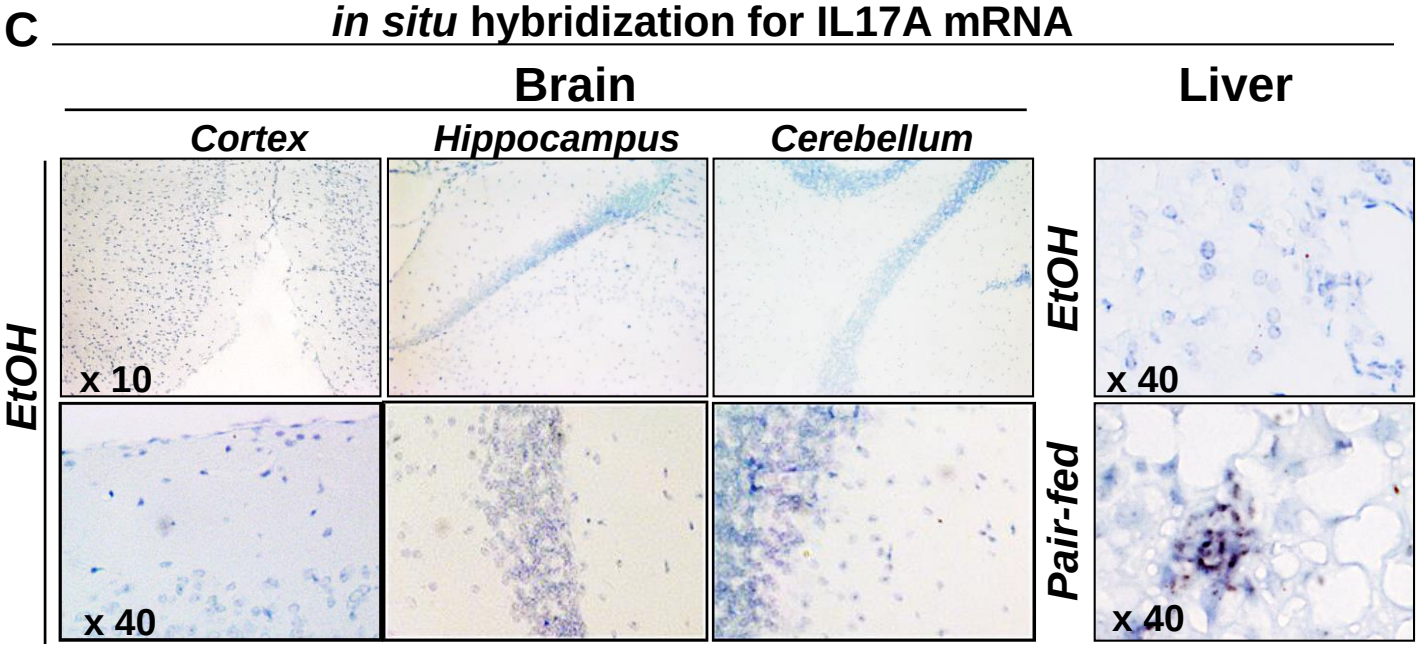
C
in situ hybridization for IL17A mRNA
Brain
Liver
Cortex
Hippocampus
Cerebellum
EtOH
x 10
x 40
EtOH
x 40
Pair-fed
x 40

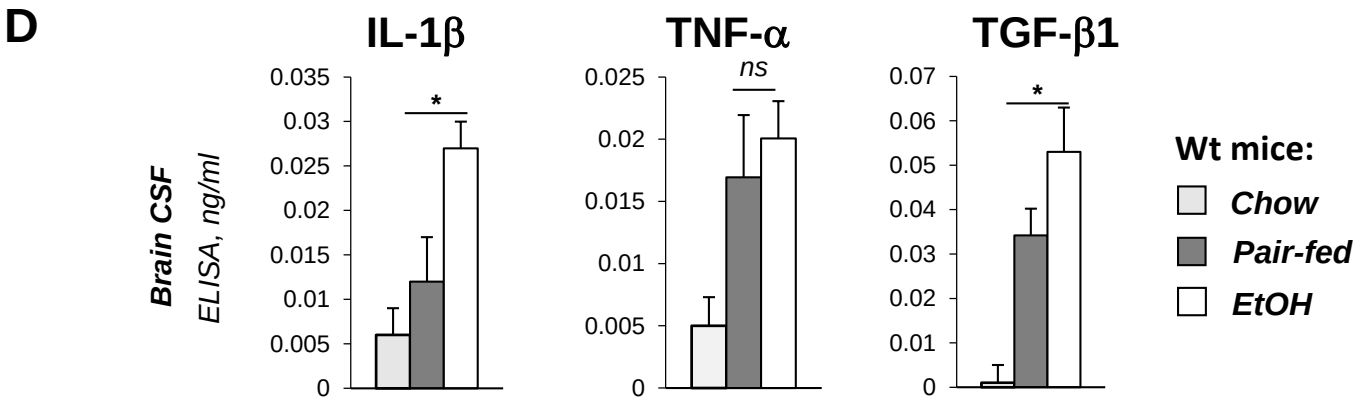
D
IL-1β
TNF-α
TGF-β1
Brain CSF
ELISA, ng/ml
0.035
0.03
0.025
0.02
0.015
0.01
0.005
0
*
0.025
0.02
0.015
0.01
0.005
0
ns
0.07
0.06
0.05
0.04
0.03
0.02
0.01
0
*
Wt mice:
Chow
Pair-fed
EtOH

Supplemental Figure 10

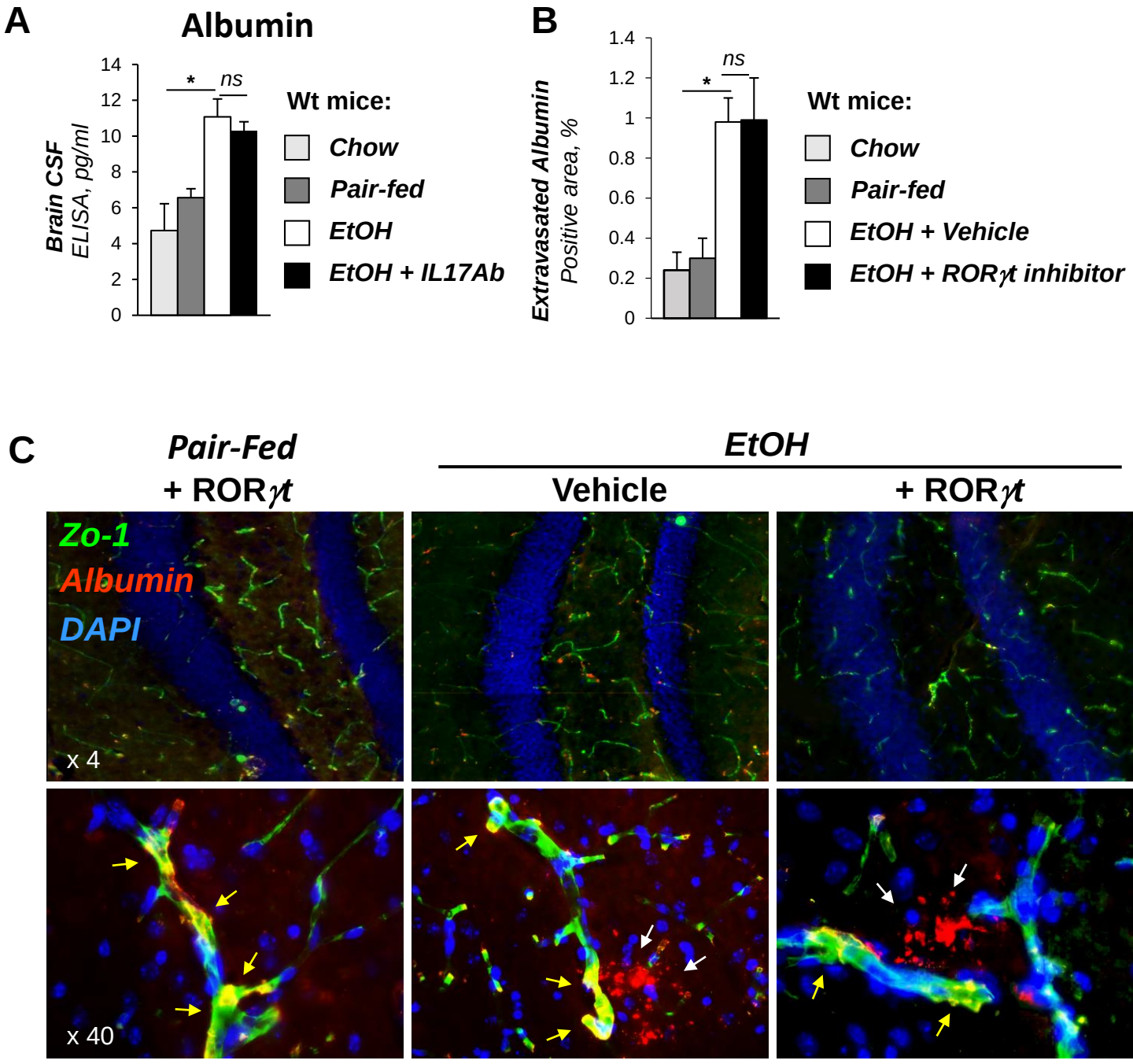

Supplemental Figure 11

A WT mice: non-dependent (Air) and alcohol-dependent (CIE)

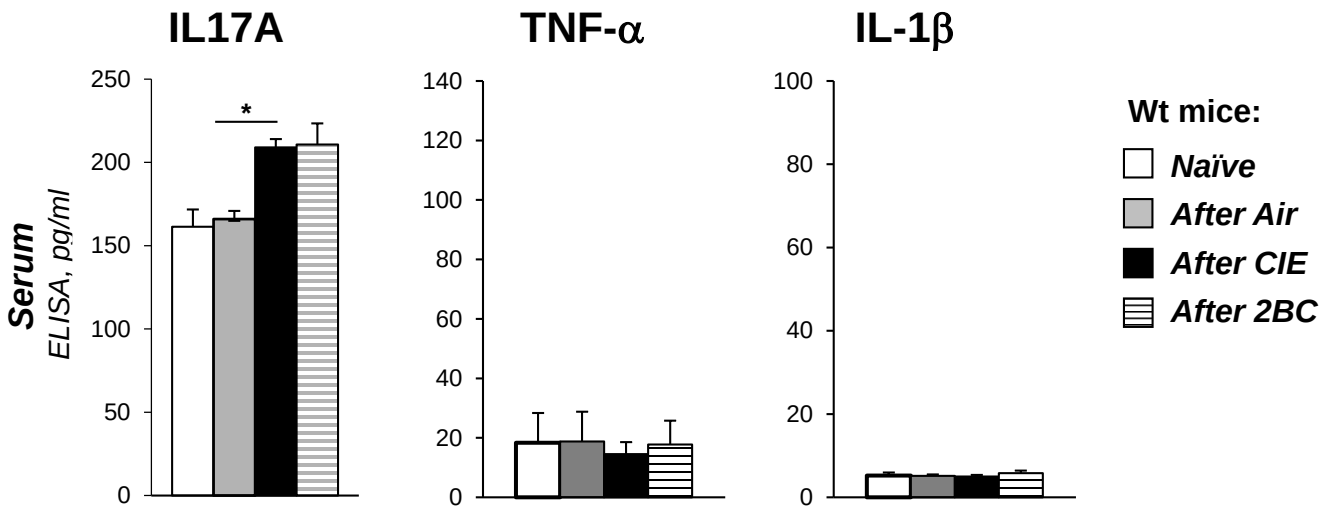

B

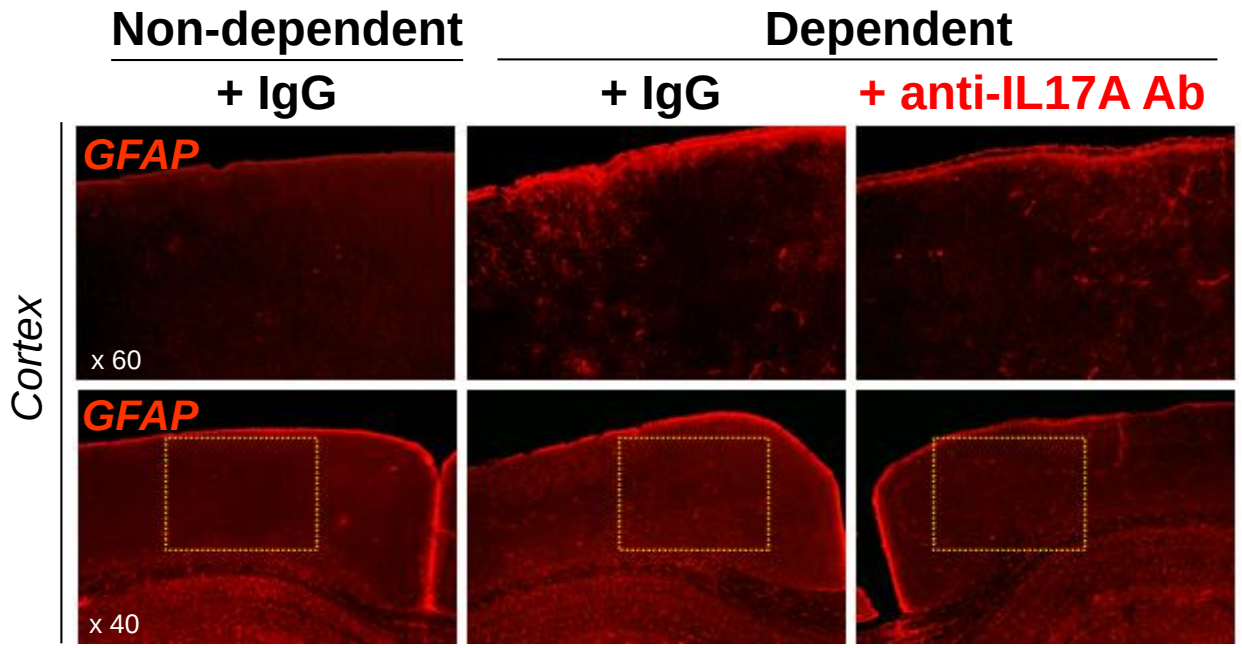

C

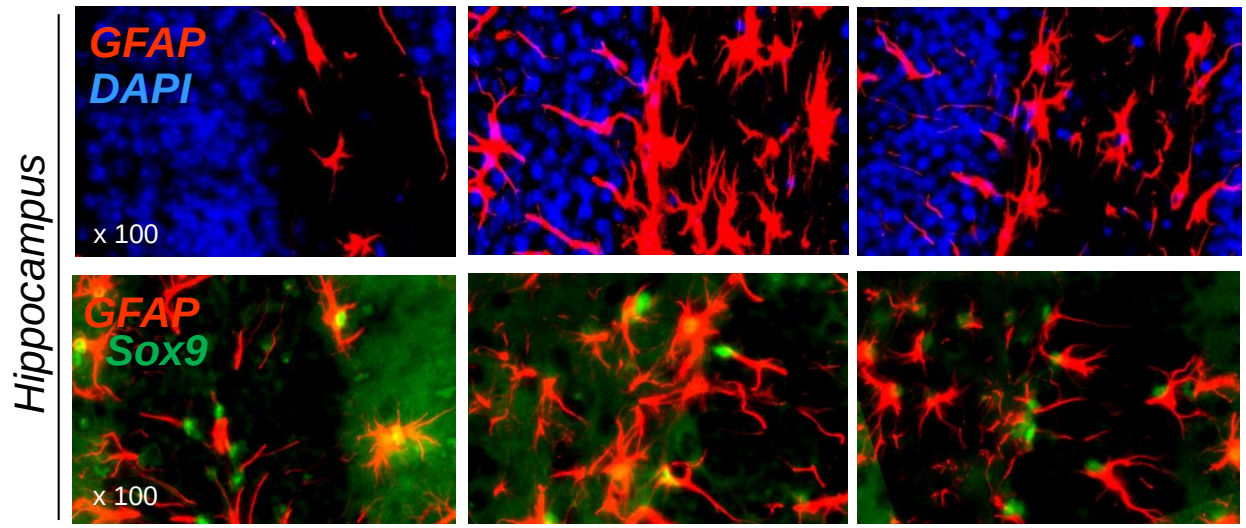

D

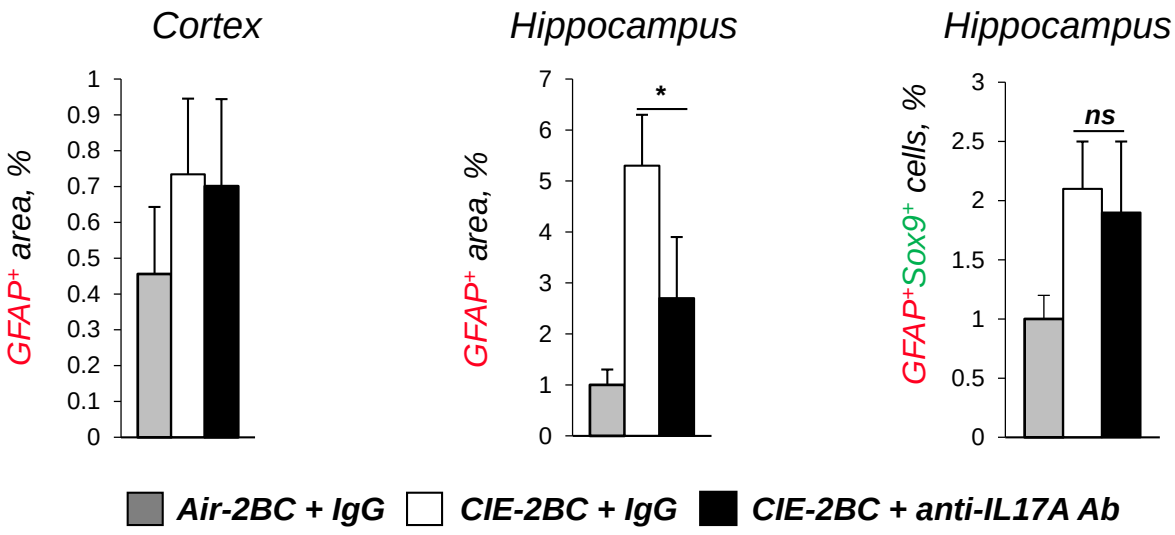
Cortex
Hippocampus
Hippocampus
GFAP+ area, %
GFAP+ area, %
GFAP+Sox9+ cells, %
*
ns
Air-2BC + IgG
CIE-2BC + IgG
CIE-2BC + anti-IL17A Ab

Supplemental Figure 12

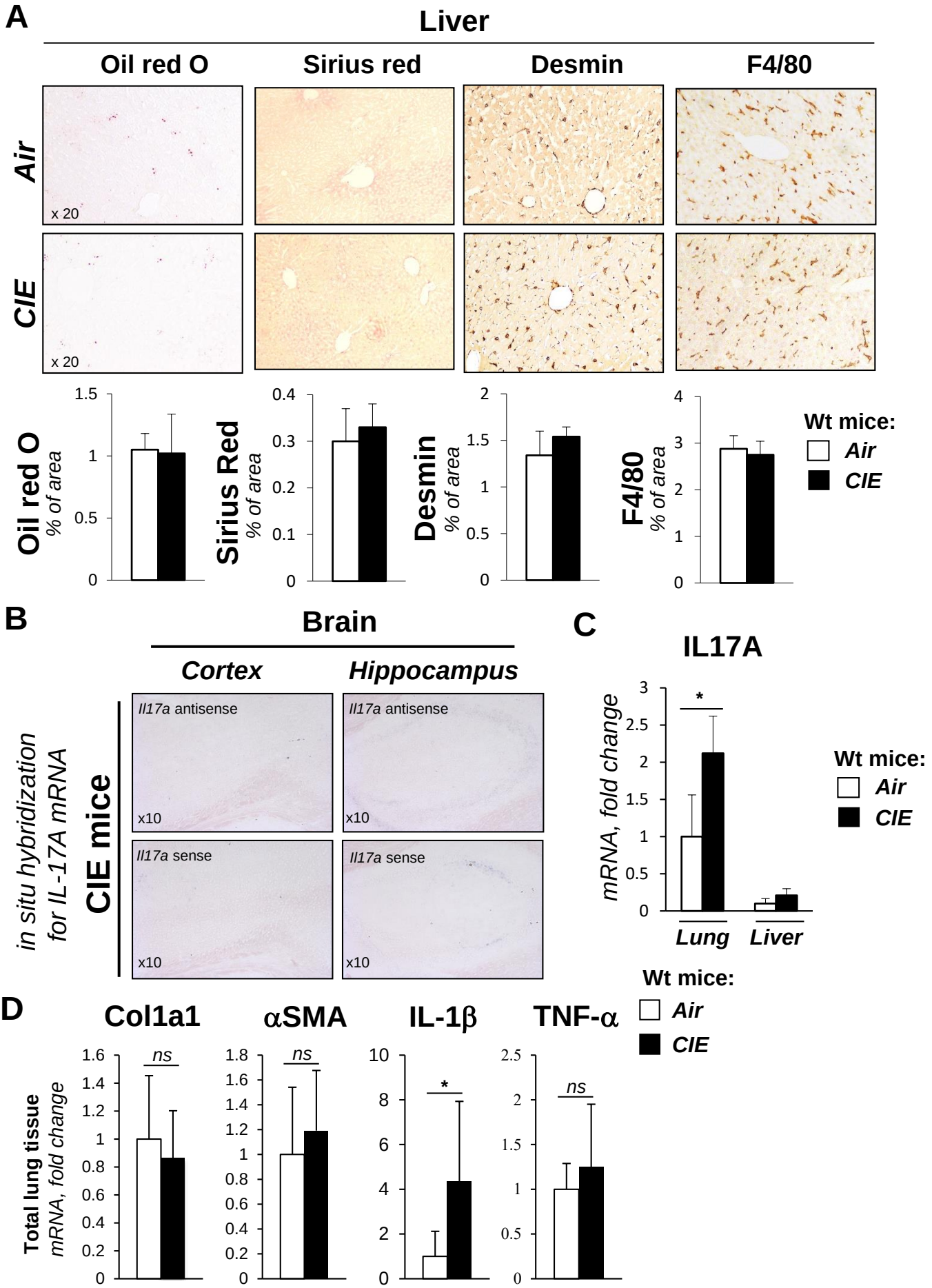

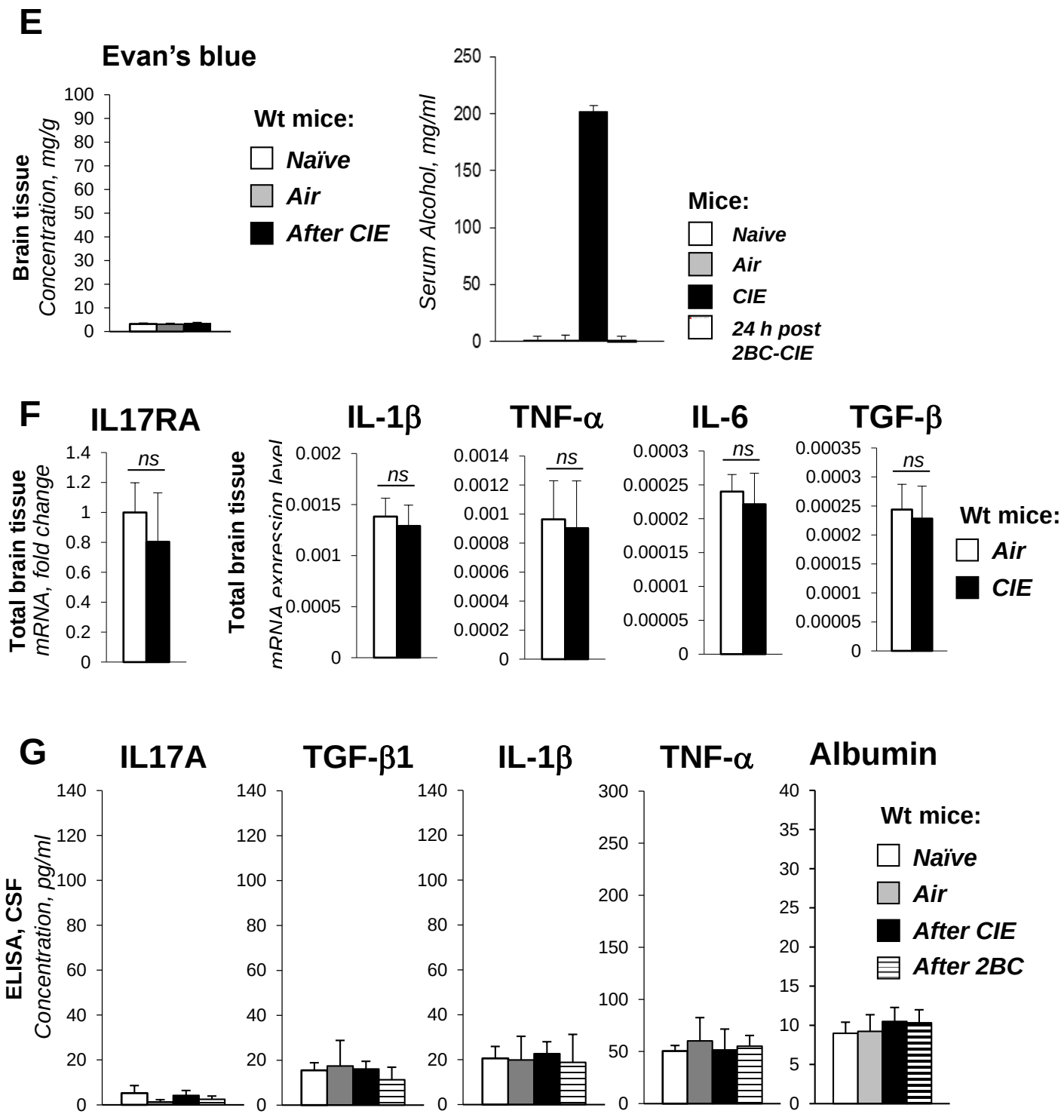
E
Evan's blue
Brain tissue
Concentration, mg/g
Wt mice:
Naïve
Air
After CIE
Serum Alcohol, mg/ml
Mice:
Naive
Air
CIE
24 h post 2BC-CIE
F
IL17RA
IL-1β
TNF-α
IL-6
TGF-β
Total brain tissue
mRNA, fold change
mRNA expression level
ns
Wt mice:
Air
CIE
G
IL17A
TGF-β1
IL-1β
TNF-α
Albumin
ELISA, CSF
Concentration, pg/ml
Wt mice:
Naïve
Air
After CIE
After 2BC

Supplemental Figure 13

CIE mice: IL17A Ab vs IgG